



# Evolution of Pb-Free and Partially Pb-Substituted Perovskite Absorbers for Efficient Perovskite Solar Cells

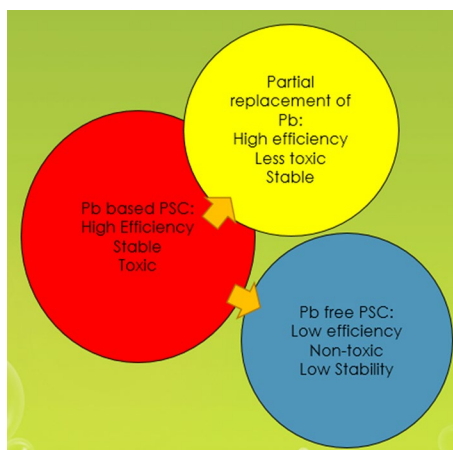
Mohd Aizat A. Wadi<sup>1,2</sup> · Towhid H. Chowdhury<sup>1,3</sup> · Idriss M. Bedja<sup>4</sup> · Jae-Joon Lee<sup>3</sup> · Nowshad Amin<sup>5</sup> · Md. Aktharuzzaman<sup>2</sup> · Ashraf Islam<sup>1</sup>

Received: 2 February 2019 / Accepted: 30 April 2019 / Published online: 18 May 2019  
© The Korean Institute of Metals and Materials 2019

## Abstract

Announced as one of the top 10 research breakthroughs in 2016, perovskite solar cells (PSC) have advanced rapidly as an established photovoltaic technology. The power conversion efficiency (PCE) of PSCs has increased quickly from 3.8% to 23.7% within a period of just 7 years. This very high PCE has been achieved by using perovskite compounds with lead (Pb) as the divalent metal ion. However, for further scale-up and commercialization, the toxicity of Pb has been identified as one of the key drawbacks for this technology. Numerous avenues for development of lead-free low-toxicity perovskite absorbers have been pursued. The unclear effect of using low-toxicity materials on optimal performance with suitable characteristics has motivated the writing of this review. Results from low-toxicity perovskite solar cells utilizing partial or complete substitution of the  $\text{Pb}^{2+}$  cation as the absorber layer are discussed in detail. Moreover, we discuss the limitations of low-toxicity absorber materials. This review summarizes the key points of film quality control, degradation effect, Pb replacement suitability, and photovoltaic performance of reported low toxicity alternate perovskite absorbers for PSCs.

## Graphical Abstract



**Keywords** Perovskite solar Cells · Pb free Perovskite solar Cells · Sn based Perovskite solar cell · Partial replacement of Pb · Efficiency · Stability

## 1 Introduction

The emergence of perovskite solar cells (PSC) occurred in 2009 with a report by Miyasaka and co-workers [1] of having achieved a power conversion efficiency (PCE) of

3.8% using  $\text{CH}_3\text{NH}_3\text{PbI}_3$  ( $\text{MAPbI}_3$ ) as the absorber in a dye-sensitized solar cell system. The use of a perovskite compound, with the formula  $\text{ABX}_3$  (A = organic cation ( $\text{CH}_3\text{NH}_3$ ), B = divalent metal ion (Pb/Sn), X = halide ion (I/Cl/Br)) instantly created a new dimension in solar cell research. Further enhancement of PSCs were observed by NG Park who reported 6.5% efficiency using  $\text{CH}_3\text{NH}_3\text{PbI}_3$  ( $\text{MAPbI}_3$ ) as the absorber [2]. Subsequently, Gratzel-Park and Snaith-Miyasaka both reported all-solid state PSCs with PCEs > 9% [3, 4]. However, a significant and reproducible fabrication process was still lacking. Numerous studies highlighted problems with deposition processes for the perovskite absorber, which affected the quality of the absorber layer (stability, smoothness,  $\text{PbI}_2$  formation) [5–7]. Some developments have included the substitution of common charge transport layers [8], the emergence of various device configurations [9], and low temperature processes [10]. In a period of just over 5 years, PSCs managed to reach 22.1% efficiency, as reported by Sang Il Seok's group, emphasizing the rapid advancement of this technology. Although the power conversion efficiency of PSCs has reached > 22% [2], issues such as (1) toxicity associated with Pb (2) long term stability and (3) highly expensive charge transport materials are hindering the commercialization of this technology.

Despite these breakthroughs in the development of PSCs, the presence of lead raises concerns about the potential environmental impact of toxic materials. With this limitation, the identification of a stable, low-toxicity halide perovskite optoelectronic material is one of the key challenges that needs to be addressed. The toxicity of Pb components is alleged to be one of the main factors that led to the collapse of the Roman Empire [11]. Elements that are members of group IV of the periodic table are regarded as the most viable replacements for Pb in perovskite materials. For the replacement of Pb, the earliest research with lead-free PSCs was reported in 2012 [12]. Fortunately, substituting Pb with Sn (tin) was inspirational due to its position in the periodic table lying within group IV. Today, however, Sn is not the sole alternative available [13–15]. Sn substitution brought the issue of stability to the attention of researchers, as the performance of the overall device is not as stable as Pb-based PSCs. This required better stability-inducing charge transport materials and better structure utilization for high efficiency devices, which has been previously reported [16, 17]. In addition, partial incorporation of non-Pb metal ions within the perovskite structure has been observed to affect the structural [18], optical [19], and photovoltaic [20] properties. The inclusion of an alternative material can instigate uncontrollable film formation, affecting the film morphology and leading to decreased photovoltaic performance [21, 22]. Meanwhile, there are few alternate materials which have been proven to assist film formation when included in the structure [23, 24]. This is due to differences in the ionic radii of each element,

which tilt/alter the crystal structure and eventually result in either better or worse quality of the film [25–27]. Hence, it is crucial to obtain an effective theoretical understanding, for practical realization of PSCs, of the effect of partial or full replacement of Pb with other alternative materials on the properties of perovskite absorbers.

Therefore, in this review, we have tried to obtain some insight into the underlying issues with the reported studies of partial and full replacement of Pb in perovskite absorbers and their effects on overall device performance. The review is comprised of two main parts. In the first part, we emphasize the effect of film crystallization and morphological and photovoltaic properties in partially substituted perovskite compounds highlighting their successful incorporation in PSCs. Based on the reported studies, in the second part of this review we discuss the full replacement of Pb with other elements. We discuss the relevant issues that have arisen by full replacement of Pb in terms of photovoltaic response and the optoelectronic effects of the corresponding PSCs. We hope that this review will guide readers in the evaluation of the potential of low toxicity and nontoxic absorbers for PSCs in future research.

## 2 Partially Substituted Perovskite Solar Cells

### 2.1 Partial Substitution of Pb by Sn

Since Sn-based PSCs show vulnerability in air, partial substitution has been considered as an alternative solution to provide improved photovoltaic response in tandem solar cells. The tunable bandgap properties of Sn/Pb-based materials are favorable for highly efficient tandem PSCs. The first partial Sn incorporation was reported by Ogomi's group in 2014 [28]. The Sn-based PSC suffered from a severe degradation mechanism which resulted in easy deterioration of the device. The substitution of  $\text{PbI}_2$  with  $\text{SnI}_2$  in the precursor retards degradation of the device. In a perovskite composition of  $\text{CH}_3\text{NH}_3\text{Sn}_x\text{Pb}_{1-x}\text{I}_3$ , with increasing values of  $x$ , the oxidation state of  $\text{Sn}^{2+}$  converges to  $\text{Sn}^{4+}$  at constant I content in the corresponding PSC. It was reported that the carrier concentrations of  $\text{CH}_3\text{NH}_3\text{SnI}_3$ ,  $\text{CH}_3\text{NH}_3\text{Sn}_{0.5}\text{Pb}_{0.5}\text{I}_3$ , and  $\text{CH}_3\text{NH}_3\text{PbI}_3$  are  $7.94 \times 10^{14} \text{ cm}^{-3}$ ,  $4.98 \times 10^{13} \text{ cm}^{-3}$ , and  $1.5 \times 10^9 \text{ cm}^{-3}$  while the drift mobilities are  $2320 \text{ cm}^2 \text{ V}^{-1} \text{ S}^{-1}$ ,  $270 \text{ cm}^2 \text{ V}^{-1} \text{ S}^{-1}$ , and  $66 \text{ cm}^2 \text{ V}^{-1} \text{ S}^{-1}$ , respectively [29]. The presence of  $\text{Sn}^{4+}$  increases the carrier concentration and drift mobility of the compound and causes it to act with metal-like properties [30]. It was observed that the presence of Pb suppressed degradation of the device in air as the absorption of  $\text{CH}_3\text{NH}_3\text{SnI}_3$  decreased by 90% in 1 min, while  $\text{CH}_3\text{NH}_3\text{Sn}_{0.5}\text{Pb}_{0.5}\text{I}_3$  retained absorption up

to 50 min with extended light absorption up to 1060 nm, red-shifted by 260 nm compared to Pb-based PSC. The exact band-edge of the material was unable to be predetermined with consistent results due to facile oxidation of  $\text{Sn}^{2+}$  to  $\text{Sn}^{4+}$  which altered the electronic properties of the material. The best performance in a mesoporous structured PSC with  $\text{CH}_3\text{NH}_3\text{Sn}_{0.5}\text{Pb}_{0.5}\text{I}_3$  composition and region-regular poly(3-hexylthiophene-2,5-diyl) (P3HT) as the hole transport material (HTM) resulted in a PCE of 4.18%, a  $V_{\text{OC}}$  of 0.42 V, fill factor (FF) of 0.50, and  $J_{\text{SC}}$  of  $20.04 \text{ mA}\cdot\text{cm}^{-2}$ . With extended absorption in the IR region,  $\text{CH}_3\text{NH}_3\text{Sn}_{0.5}\text{Pb}_{0.5}\text{I}_3$  is regarded as a potential material for the bottom cell in tandem solar cells. Kanatzidis et al. reported higher efficiency of partially Sn-substituted mesoporous PSC by incorporating 25% Sn in  $\text{CH}_3\text{NH}_3\text{Sn}_{0.25}\text{Pb}_{0.75}\text{I}_3$  [31]. The replacement of P3HT with Spiro-OMeTAD resulted in a better HTM [32]. No separate phase was observed for Sn/Pb, and the corresponding  $\text{CH}_3\text{NH}_3\text{Sn}_{0.25}\text{Pb}_{0.75}\text{I}_3$  absorber provided homogenous distribution of Pb and Sn elements throughout the film. The optimized PSC only incorporated 25% of Sn compared to Ogomi's 50%. The bandgap for 25% and 50% Sn substitution resulted in 1.24 eV and 1.17 eV respectively. Although the 50% Sn film showed better film coverage with smaller crystallite growth, the increased amount of  $\text{Sn}^{4+}$  reduced the  $V_{\text{OC}}$  from 0.728 V to 0.584 V. The FF also increased as the amount of Pb inclusion in the perovskite compound was increased. This is due to the possibility of Pb inclusion for formation of crystals, favoring high coverage and quality film [7]. With  $\text{CH}_3\text{NH}_3\text{Sn}_{0.25}\text{Pb}_{0.75}\text{I}_3$  as the absorber, a PCE of 7.37% was achieved with  $J_{\text{SC}} = 15.82 \text{ mA}\cdot\text{cm}^{-2}$ , and  $\text{FF} = 0.64$ . Jen et al. reported the first planar Sn/Pb PSC by reducing the Sn content to only 15% in order to limit  $V_{\text{OC}}$  reduction [33]. The inclusion of Cl within the absorber resulted in  $\text{CH}_3\text{NH}_3\text{Pb}_{1-x}\text{Sn}_x\text{I}_{3-x}\text{Cl}_x$ . With a structure of ITO/PEDOT:PSS/ $\text{CH}_3\text{NH}_3\text{Pb}_{1-x}\text{Sn}_x\text{I}_{3-x}\text{Cl}_x$ /Phenyl-C61-butryic acid methyl ester (PCBM)/Bis-Salt/Ag, the PCE exceeded 10%. With partial introduction of Sn, the film had continuous and uniform coverage ( $\sim 97\%$ ). The optimum amount of  $\text{Sn}^{2+}$  influences nucleation during formation of the film. The inclusion of  $\text{Sn}^{2+}$  also extended the absorption range, red-shifting the normal Pb-based PSC absorption by  $\sim 100 \text{ nm}$  (from 800 nm to  $\sim 900 \text{ nm}$ ) simultaneously with an increase in the material's absorbing ability at 600–800 nm wavelength (Fig. 1b). Although previous reported studies [29, 31] showed the unconfirmed exact band-edge location of the materials due to intrinsic defects caused by  $\text{Sn}^{2+}$  oxygenation, this work highlighted the well-matched bandgap of the proposed electronic structure. Therefore, the role of Pb in retarding premature degradation of lead-free perovskite is highly evidential. Incorporation of chlorine has been identified with beneficial

impacts in Pb-based PSCs as reported by previous studies [34, 35]. Deploying the  $\text{CH}_3\text{NH}_3\text{Pb}_{0.85}\text{Sn}_{0.15}\text{I}_{3-x}\text{Cl}_x$  composition in an inverted planar structure, a PCE of up to 10.1% was reported with  $J_{\text{SC}} = 19.1 \text{ mA}\cdot\text{cm}^{-2}$ ,  $V_{\text{OC}} = 0.76 \text{ V}$ , and  $\text{FF} = 0.66$ .

The highest efficiency for a mixed Sn/Pb-based PSC has been reported by Yanfa Yan's group with a PCE of 15% [23]. Sang Il Seok's group [36] reported higher stability of formamidinium tin iodide ( $\text{FASnI}_3$ ) in comparison to  $\text{MASnI}_3$  perovskite compound [10, 37]. The usage of  $(\text{FASnI}_3)_{1-x}(\text{MAPbI}_3)_x$  precursor solution where  $\text{FASnI}_3$  was mixed with 10 mol % of  $\text{SnF}_2$  additive yielded beneficial aspects. The  $(\text{FASnI}_3)_{1-x}(\text{MAPbI}_3)_x$  precursor results in improved crystalline film quality with a root mean square (RMS) roughness of 9.5 nm compared to that of pure  $\text{FASnI}_3$  (14.8 nm). The  $(\text{FASnI}_3)_{0.6}(\text{MAPbI}_3)_{0.4}$  film showed smaller and homogenous grain size which led to a compact high coverage layer (Fig. 2). The  $(\text{FASnI}_3)_{1-x}(\text{MAPbI}_3)_x$  precursor-based PSC showed high reproducibility with the average efficiency of 50 cells at  $14.39 \pm 0.33\%$ . It is also worth noting that the bandgap of the optimum  $(\text{FASnI}_3)_{0.6}(\text{MAPbI}_3)_{0.4}$  film was 1.2 eV which deviates slightly from previously reported results. This phenomenon was attributed to the inclusion of the FA cation with a lower bandgap than that of the MA cation in the corresponding perovskite films [38]. The inverted planar structure also avoided any salt additive usage in the perovskite layer. With a structure of ITO/PEDOT:PSS/ $(\text{FASnI}_3)_{0.6}(\text{MAPbI}_3)_{0.4}/\text{C}_{60}/\text{Bathocuproine (BCP)}/\text{Ag}$ , the best Sn/Pb-based PSC achieved up to 15.08% PCE with photovoltaic parameters of  $J_{\text{SC}} = 26.86 \text{ mA}\cdot\text{cm}^{-2}$ ,  $V_{\text{OC}} = 0.795 \text{ V}$ , and  $\text{FF} = 0.706$ . Despite the fact that the ratio of Sn to Pb was 6:4, higher than any reported results, the  $V_{\text{OC}}$  of the devices was quite remarkable. Negligible hysteresis ( $\sim 0.08\%$ ) provided by the corresponding PSC further emphasizes the high quality of the film obtained from the novel engineered precursor solution. This was attributed to the least amount of any intrinsic or band-edge defect which acted as the main factor in nonradiative recombination [39].

Hillhouse's group reported the first wide bandgap Sn/Pb PSC [40] in inverted planar structure with ITO/PEDOT:PSS/ $\text{MAPb}_{1-x}\text{Sn}_x(\text{I}_{1-y}\text{Br}_y)_3/\text{PCBM}/\text{Bis-C}_{60}/\text{Ag}$ . In this work, partial replacement of I with Cl or Br enhanced the bandgap of the perovskite absorber material [41–43]. Compounds with the formula  $\text{MAPb}_{1-x}\text{Sn}_x(\text{I}_{1-y}\text{Br}_y)_3$  were used for designing a stable and wider bandgap (1.7 eV) with the Sn content fixed at 25%. The presence of 25% Sn content in the corresponding perovskite films displayed improved film morphology and successfully prevented phase segregation of  $\text{MAPb}(\text{I}_{1-x}\text{Br}_x)_3$  [44, 45]. The optimized cell composition of  $\text{MAPb}_{0.75}\text{Sn}_{0.25}(\text{I}_{0.4}\text{Br}_{0.6})_3$ -based PSC achieved up to 12.59% PCE with photovoltaic parameters of  $J_{\text{SC}} = 15.52 \text{ mA}\cdot\text{cm}^{-2}$ ,  $V_{\text{OC}} = 1.04$  and  $\text{FF} = 0.78$ . The cell was relatively stable, maintaining its 95% initial efficiency

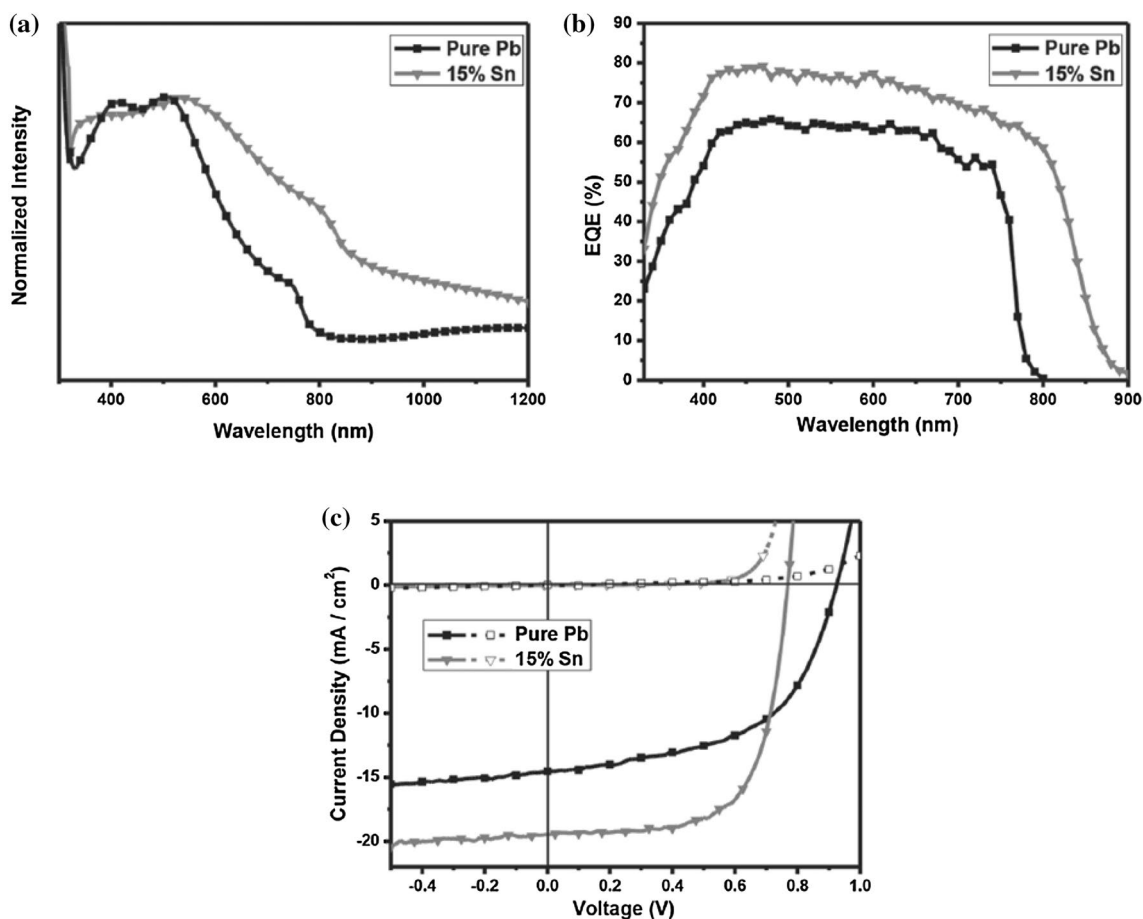


**Fig. 1** Comparison of MAPbI<sub>3</sub> and MA Pb<sub>0.85</sub>Sn<sub>0.15</sub>I<sub>3-x</sub>Cl<sub>x</sub> optical and photovoltaic properties in terms of: **a** UV–Vis absorption spectra, **b** EQE results and **c** J–V curves. Reproduced with permission [33] Copyright 2014 John Wiley & Sons

in a dark and inert condition for 30 days (Fig. 3). The PSC retained 94% of its initial efficiency under a thermal stress of 85 °C for 24 h.

## 2.2 Partial Substitution of Pb by Hg and In

Despite the fact that Sn has received most of the attention either in lead-free or partially-substituted perovskite absorbers, numerous attempts have been made to substitute other elements. The Goldschmidt model provides theoretical simulation which estimates the stability of the ABX<sub>3</sub> perovskite by comparing the ionic radius of each element [46]. Several elements are compatible when the elements of A = MA and X = I/Br are fixed [47–49]. A group from Moscow State University worked with a series of elements by partially substituting Pb ions [50]. The work highlighted mainly Pb replacement by Hg<sup>2+</sup> while Cd<sup>2+</sup>, Zn<sup>2+</sup>, Fe<sup>2+</sup>, Ni<sup>2+</sup>, Co<sup>2+</sup>, In<sup>3+</sup>, Bi<sup>3+</sup>, Sn<sup>4+</sup>, and Ti<sup>4+</sup> were also studied to observe their potential usage in PSCs. The optical and photovoltaic properties of each partially substituted element as perovskite absorbers were investigated with a composition of

MAPb<sub>0.9</sub>B<sub>0.1</sub>I<sub>3</sub>, where B is the substituted element. Substitution with a univalent metal ion (Cu<sup>+</sup>, Ag<sup>+</sup>) promoted formation of interstate trap states within the band-edge. Amongst all the examined elements, only Hg<sup>2+</sup> enhanced the PCE of the PSC while the others showed decreased performance (Fig. 4a, b). The ionic radius of Hg<sup>2+</sup> is around 1.33 Å, which is quite similar to that of Sn<sup>2+</sup> (1.35 Å). Therefore, perturbation in the crystal lattice of the perovskite which is susceptible to an interstate defect with other elements is less likely to occur as the ionic radii of the Hg<sup>2+</sup> and Pb<sup>2+</sup> are similar. The potential of Hg<sup>2+</sup> in PSC was also confirmed as the absorption spectra of the materials were enhanced with Hg<sup>2+</sup> inclusion. With an increased fraction of Hg<sup>2+</sup> (> 30%), phase segregation started to occur and unfavorable co-crystallization occurred. A further increment of the Hg<sup>2+</sup> fraction up to 70% resulted in massive deterioration of the light absorption properties at 350–570 nm while the “perovskite” band at 650–800 nm was still present as the fraction was increased. Although the ionic radius of Hg<sup>2+</sup> is smaller than that of Pb<sup>2+</sup>, the phase structure showed that Hg<sup>2+</sup> can successfully reside in the compound without distorting the

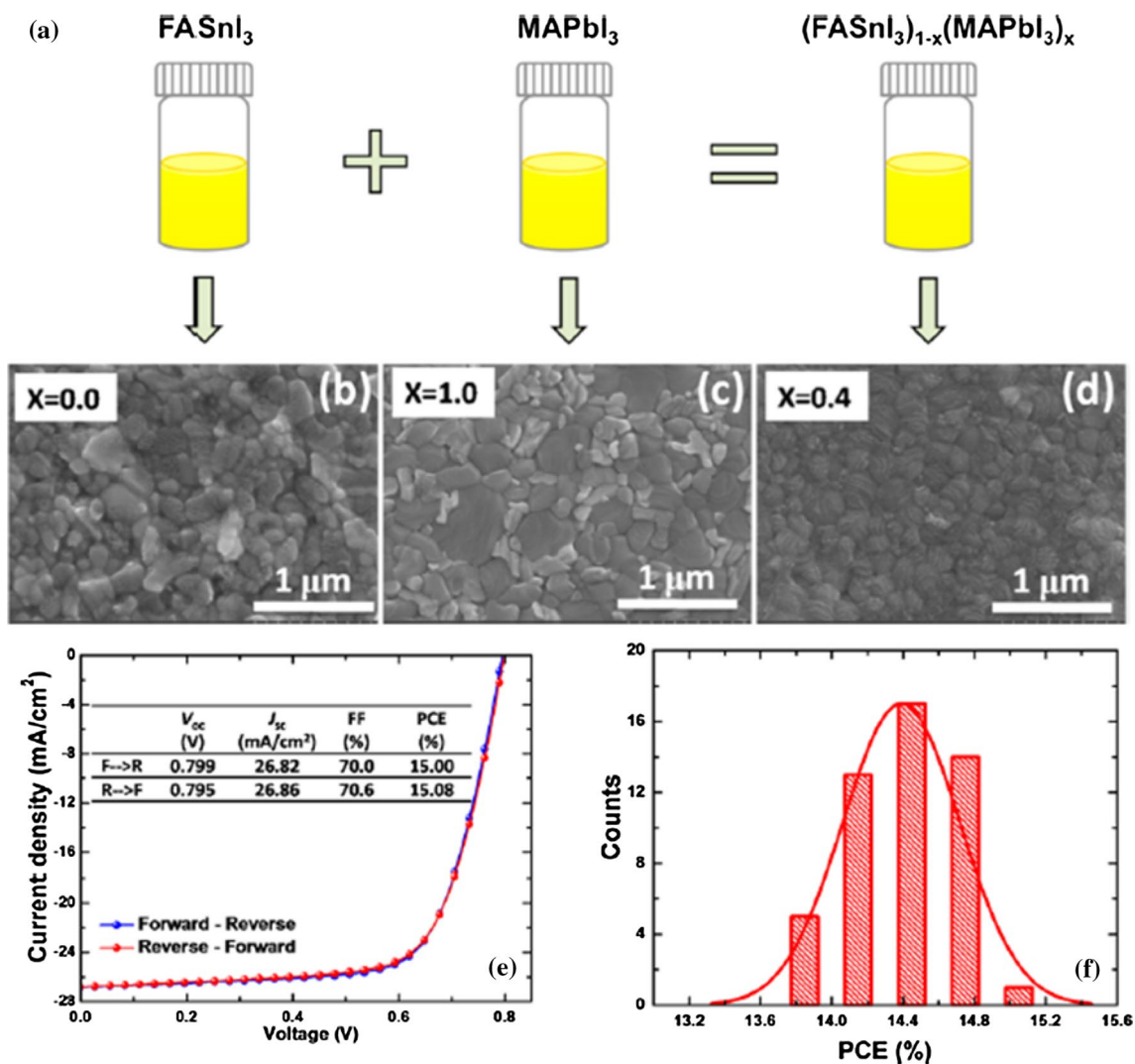


**Fig. 2** a Schematic formation of  $(\text{FASnI}_3)_{1-x}(\text{MAPbI}_3)_x$  precursor solution, b–d SEM surface images of  $\text{FASnI}_3$ ,  $\text{MAPbI}_3$  and  $(\text{FASnI}_3)_{1-x}(\text{MAPbI}_3)_x$ , respectively, e  $(\text{FASnI}_3)_{0.6}(\text{MAPbI}_3)_{0.4}$  J-V

curve in forward and reverse scan, f Histogram of collected 50 PCEs using  $(\text{FASnI}_3)_{0.6}(\text{MAPbI}_3)_{0.4}$  composition. Reproduced with permission [23] Copyright 2016, American Chemical Society

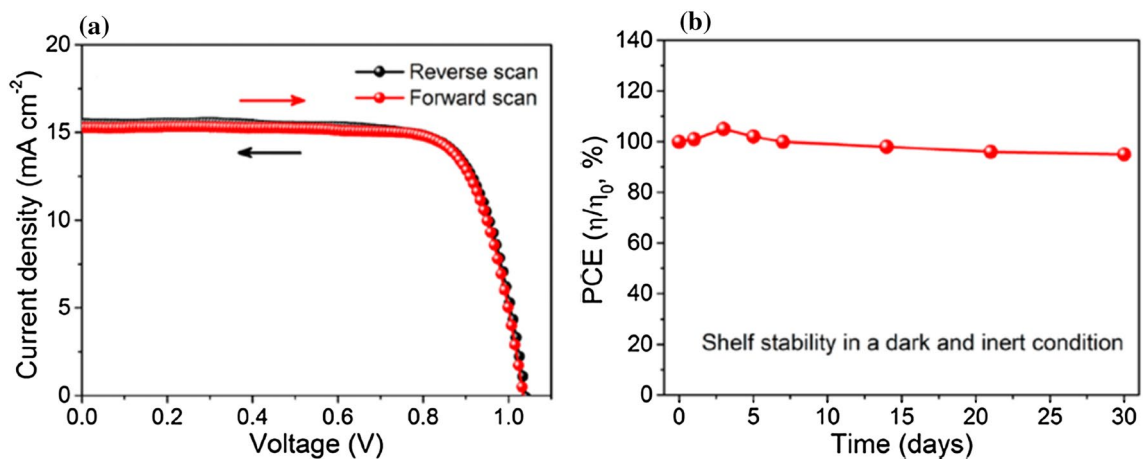


**Fig. 3** a J-V Curve of  $\text{MAPb}_{0.75}\text{Sn}_{0.25}(\text{I}_{0.4}\text{Br}_{0.6})_3$  and b Best cell stability test in a dark and inert condition for 30 days. Reproduced with permission [40] Copyright 2016, American Chemical Society



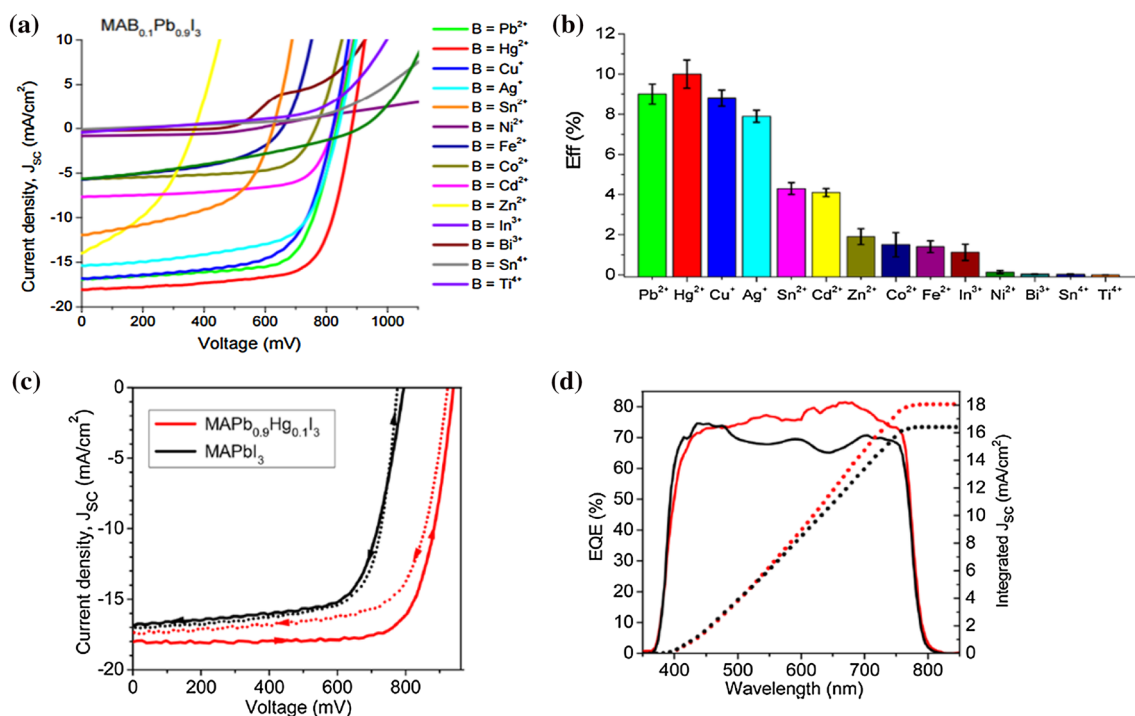


**Fig. 4** **a** J-V curve of each substituted element in  $\text{MAB}_{0.1}\text{Pb}_{0.9}\text{I}_3$  composition **b** PCE of various substituted elements; comparison of photovoltaic properties between  $\text{MAPb}_{0.9}\text{Hg}_{0.1}\text{I}_3$  and pristine  $\text{MAPbI}_3$  in

**c** J-V curves and **d** EQE Spectra. Reproduced with permission [50] Copyright 2016, American Chemical Society

perovskite crystal structure. Obvious enhancement in external quantum efficiency (EQE) near the absorption peaks of  $\text{MAPb}_{0.9}\text{Hg}_{0.1}\text{I}_3$  further boosted the photovoltaic performance of Pb/Hg based PSC (Fig. 4d). The  $\text{MAPb}_{0.9}\text{Hg}_{0.1}\text{I}_3$  cell achieved the best PCE of 13.0%, attaining values of  $J_{sc} = 18.1 \text{ mA}\cdot\text{cm}^{-2}$ ,  $V_{oc} = 0.94 \text{ V}$ , and  $FF = 0.764$ . The inclusion of  $\text{Hg}^{2+}$  assists film nucleation as it affects the carrier mobility in the corresponding PSC (Fig. 4c).

Liang-Sheng Liao et al. fabricated high efficiency PSCs with partial substitution of indium in the Pb-based absorber [24]. A very small amount of  $\text{In}^{3+}$  addition resulted in improvement of optical, film and photovoltaic properties. Even by using a pure  $\text{PbCl}_2$  route (Fig. 5a), large and high quality grains ( $2\text{--}5 \mu\text{m}$ ) can be obtained, but pinhole formation cannot be effectively suppressed [51, 52]. The effect of pinhole formation can be observed in the FF value of the devices:  $\text{PbCl}_2$  (0.72) compared to  $\text{InCl}_3$  (0.78) mixed perovskite films. Even though the average crystal size obtained with the  $\text{PbCl}_2$  (85%)- $\text{InCl}_3$  (15%) route is smaller (Fig. 5b), the film has a more compact nature and covers 95.4% of the film surface. Multiple phases of crystal orientation formed by  $\text{MAPb}_{1-x}\text{In}_x\text{I}_3\text{Cl}_x$  also contribute to a superior capability to transport charge carriers. Hole mobility and electron mobility of the film increased significantly from  $0.45 \text{ cm}^2 \text{ V}^{-1} \text{ S}^{-1}$  and  $0.65 \text{ cm}^2 \text{ V}^{-1} \text{ S}^{-1}$  to  $1.45 \text{ cm}^2 \text{ V}^{-1} \text{ S}^{-1}$  and  $0.65 \text{ cm}^2 \text{ V}^{-1} \text{ S}^{-1}$ , respectively. A controlled amount

of indium inclusion in  $\text{MAPb}_{1-x}\text{In}_x\text{I}_3\text{Cl}_x$  and the use of an inverted planar structure with the configuration ITO/PEDOT: PSS/ $\text{PC}_{61}\text{BM}$ /Bphen/Ag enhanced photovoltaic parameters significantly. The best device showed impressive photovoltaic properties, with  $J_{sc} = 21.90 \text{ mA}\cdot\text{cm}^{-2}$ ,  $V_{oc} = 1.03 \text{ V}$ , and  $FF = 0.78$ , leading to a PCE of 17.55% (Fig. 5c). The enhancement of PCE was contributed to by lower pinhole formation upon  $\text{InCl}_3$  inclusion within the perovskite precursor solution at an optimum amount. Indium was also successfully partially substituted for Pb. The overall stability of the  $\text{MAPb}_{1-x}\text{In}_x\text{I}_3\text{Cl}_x$  based PSC measured for 350 h was higher than that of  $\text{MAPbI}_3\text{Cl}_{1-x}$ . However, due to lack of reproducibility of this work, a proper explanation for  $\text{InCl}$  addition in the absorber is lacking. This issue may be related to the chlorine effect in mixed halide perovskites, as mentioned in previous reports [42, 52, 53], where using only chlorine for the halide induced better crystal formation for high quality perovskite films.

### 2.3 Partial Substitution of Pb by $\text{Sr}^{2+}$

Bolink et al. investigated partial inclusion of homovalent cations using strontium ( $\text{Sr}^{2+}$ ). Previous work on partial inclusion of  $\text{Sr}^{2+}$  in  $\text{MAPbI}_3$  powder demonstrated the ability of Sr to be a possible candidate due to favorable optical and electronic properties and favorable doping

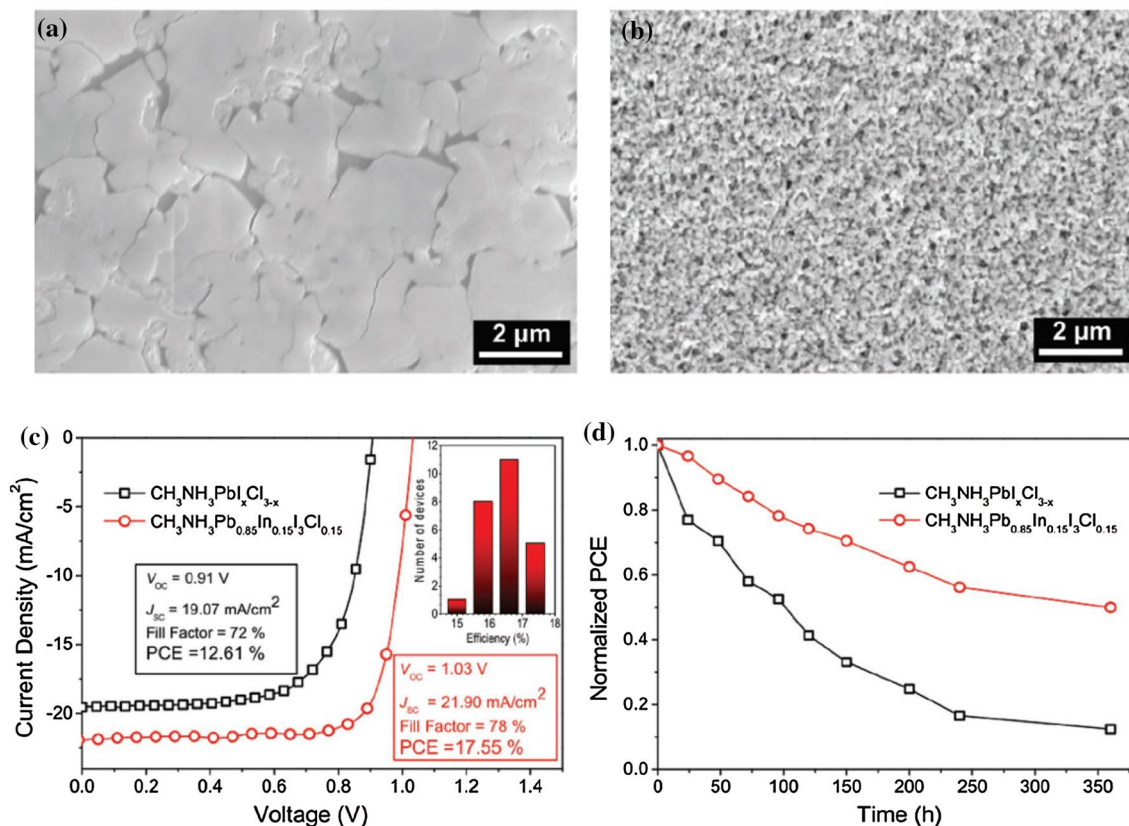


**Fig. 5** **a** SEM Surface image for  $\text{MAPbI}_{3-x}\text{Cl}_x$ ; **b** SEM Surface image for  $\text{MAPb}_{0.85}\text{In}_{0.15}\text{I}_3\text{Cl}_{0.15}$ ; **c** Comparison of I-V curve with and without inclusion of Indium; and **d** Normalized PCE values ver-

sus exposed time to air. Reproduced with permission [24] Copyright 2016 John Wiley & Sons

effects in perovskite absorber material. An inverted planar structured PSC with configuration ITO/Poly(3,4-ethylenedioxythiophene) doped with (polystyrene sulfonate) (PEDOT:PSS)/ $\text{MAPbI}_3\text{:Sr}^{2+}$ /Indene- $\text{C}_{60}$ -propionic acid hexyl ester (IPH)/Ba-Ag has been successfully evaluated [54]. Densely packed perovskite crystallites were observed with the addition of 2%  $\text{Sr}^{2+}$ , which resulted in excellent flat and homogenous films. Compared to pristine  $\text{MAPbI}_3$ , the average domain crystal size of the film was reduced from 100–200 nm to only 20–100 nm for a Pb-Sr absorber. This enabled  $\text{MAPbI}_3\text{:Sr}^{2+}$  films with increased continuity and prevented any formation of pinholes on the surface of the corresponding film. The effect of  $\text{Sr}^{2+}$  addition can be clearly observed in surface SEM images of the  $\text{MAPbI}_3\text{:Sr}^{2+}$  absorber (Fig. 6a–c). However, not only do the crystals undergo obvious changes in the crystallization process as observed in SEM surface images, but also changes in electronic properties as the amount of Sr varies. These changes are suspected to be due to a change of Density of States (DOS) as the author found that the valence band maximum (VBM) of 5%  $\text{Sr}^{2+}$  is at 0.5 eV below the Fermi level ( $E_f$ ). On the other hand, the VBM of 2%  $\text{Sr}^{2+}$  film is at 0.6 eV below  $E_f$ .

The current density of Sr-doped perovskite increases substantially up to  $18 \text{ mA}\cdot\text{cm}^{-2}$  as the percentage of  $\text{Sr}^{2+}$  was increased to 2%. The improvement of  $J_{\text{SC}}$  may be related to an improvement in carrier lifetime ( $> 40 \mu\text{s}$ ) (Fig. 6f, g). Meanwhile, the  $V_{\text{OC}}$  of the device decreased to 950 mV compared to 1 V with pure  $\text{MAPbI}_3$ . This significant drop in  $V_{\text{OC}}$  value was accompanied by a significant increase in FF value of the overall device from 77% to 85% by partial substitution of Pb with Sr. The best device with an optimum amount of 2%  $\text{Sr}^{2+}$  reached a PCE value of 15% with  $J_{\text{SC}} = 18 \text{ mA}\cdot\text{cm}^{-2}$ ,  $V_{\text{OC}} = 0.95 \text{ V}$ , and  $\text{FF} = 0.85$ . Interestingly, the formation of a thin layer of  $\text{Sr}(\text{C}_2\text{H}_3\text{O}_2)_2$  was observed at the interface between the perovskite absorber and the corresponding HTM. The layer however did not interrupt charge carrier extraction but instead altered the work function of the material and provided better movement of carriers throughout the device. This tradeoff can be seen clearly by the decreasing value of  $V_{\text{OC}}$  at the same time as a substantial increase in  $J_{\text{SC}}$ .

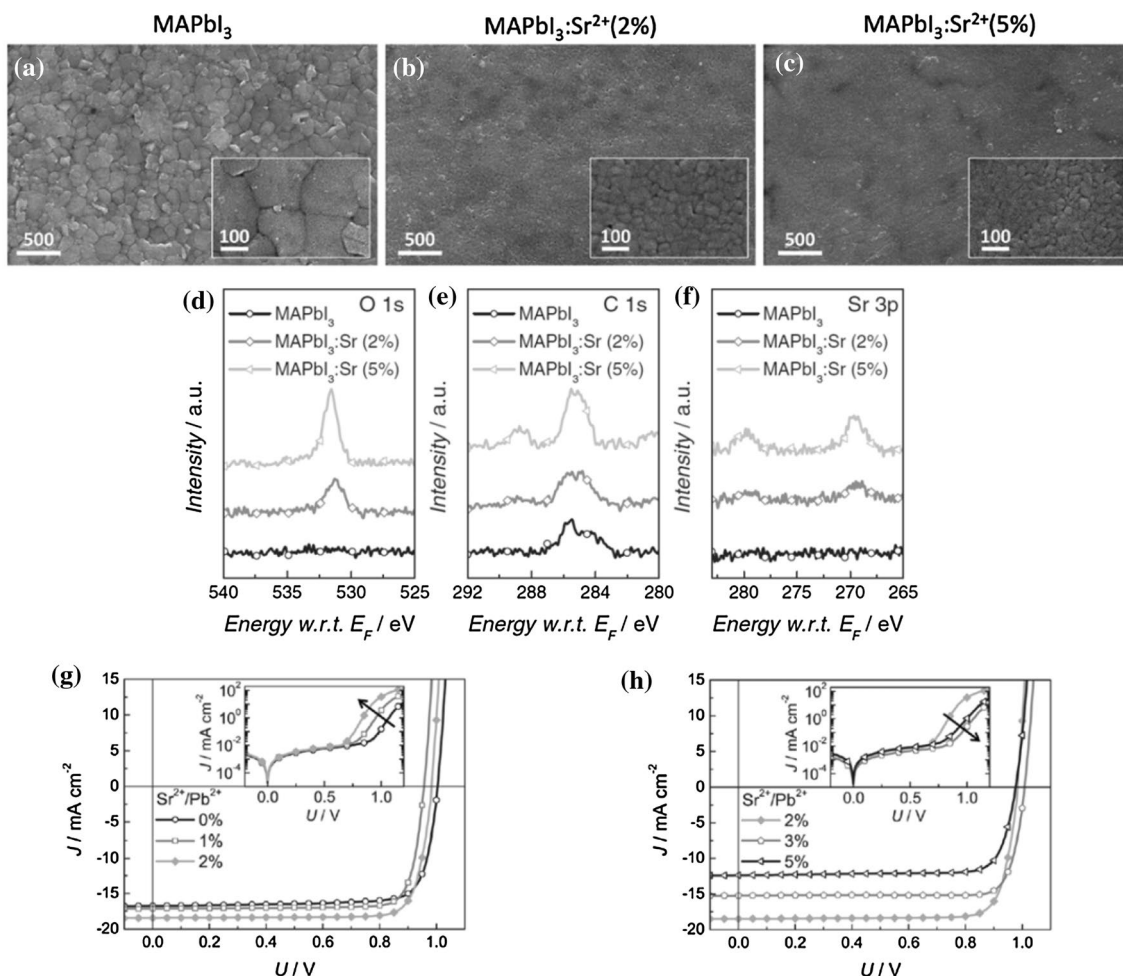


**Fig. 6** Effect of different amounts of  $\text{Sr}^{2+}$  on **a–c** absorber surface morphology by SEM surface images, **d–f** Element content by XPS Spectra and **g, h** Photovoltaic parameters by J-V curves. Reproduced with permission [54] Copyright 2016 John Wiley & Sons

## 2.4 Partial Substitution of Pb by Sb

For the first time, n-doping using Antimony ( $\text{Sb}^{3+}$ ) incorporation into perovskite absorber has been reported by Han et al. [27]. The n-doping of  $\text{Sb}^{3+}$  resides perfectly in the perovskite crystal phase with the chemical formula  $\text{MAPb}_{1-x}\text{Sb}_{2x/3}\text{I}_3$ . Compared to Sr partial substitution, no impurity phase was detected even with 8% incorporation of  $\text{Sb}^{3+}$  into  $\text{MAPb}_{1-x}\text{Sb}_{2x/3}\text{I}_3$ . Inclusion of Sb at 0% to 25% in the  $\text{MAPb}_{1-x}\text{Sb}_{2x/3}\text{I}_3$  complex results in a sharp absorption increase up to 800 nm while a further increment of  $\text{Sb}^{3+} > 25\%$  inhibits a gradual decrease in the absorption (Fig. 7a). This is due to complete substitution of  $\text{Sb}^{3+}$  which undergoes transition from a direct to an indirect bandgap [55]. The valence band maximum (VBM) and conduction band minimum (CBM) of the  $\text{MAPb}_{1-x}\text{Sb}_{2x/3}\text{I}_3$  film fluctuate depending on the amount of  $\text{Sb}^{3+}$  incorporation in the film. The VBM of the film shifted from 0 eV in vacuum as the amount of antimony inclusion increased (Fig. 7b). This

is due to the Fermi level, as the n-doping process leads to enhancement of the film bandgap. The  $\text{Sb}^{3+}$  amount included by 1% doping increased the bandgap to  $\sim 1.57$  eV. The best cell performance obtained using 1%  $\text{Sb}^{3+}$  inclusion in a PSC was a PCE of 15.6%, ( $J_{\text{SC}} = 21.82 \text{ mA cm}^{-2}$ ,  $V_{\text{OC}} = 0.985 \text{ V}$  and  $\text{FF} = 0.692$ ) compared to pristine perovskite film with a PCE of only 13.1% (Fig. 7c).

## 2.5 Partial Substitution of Pb by Zn

Shengzhong Liu et al. introduced  $\text{Zn}^{2+}$  as a doping element for the perovskite compound in a PSC [56]. Unlike other partial substitutions,  $\text{Zn}^{2+}$ -doped perovskite absorber acted as a catalyst in assisting crystal phase formation. XRD characterization of the doped PSC displays no impurity of  $\text{PbI}_2$  present in the samples. The perovskite structure was altered slightly as some Pb ions were substituted with Zn ions with a smaller radius. Figure 8a–c shows FESEM surface images of the Zn-doped perovskite compound at varied



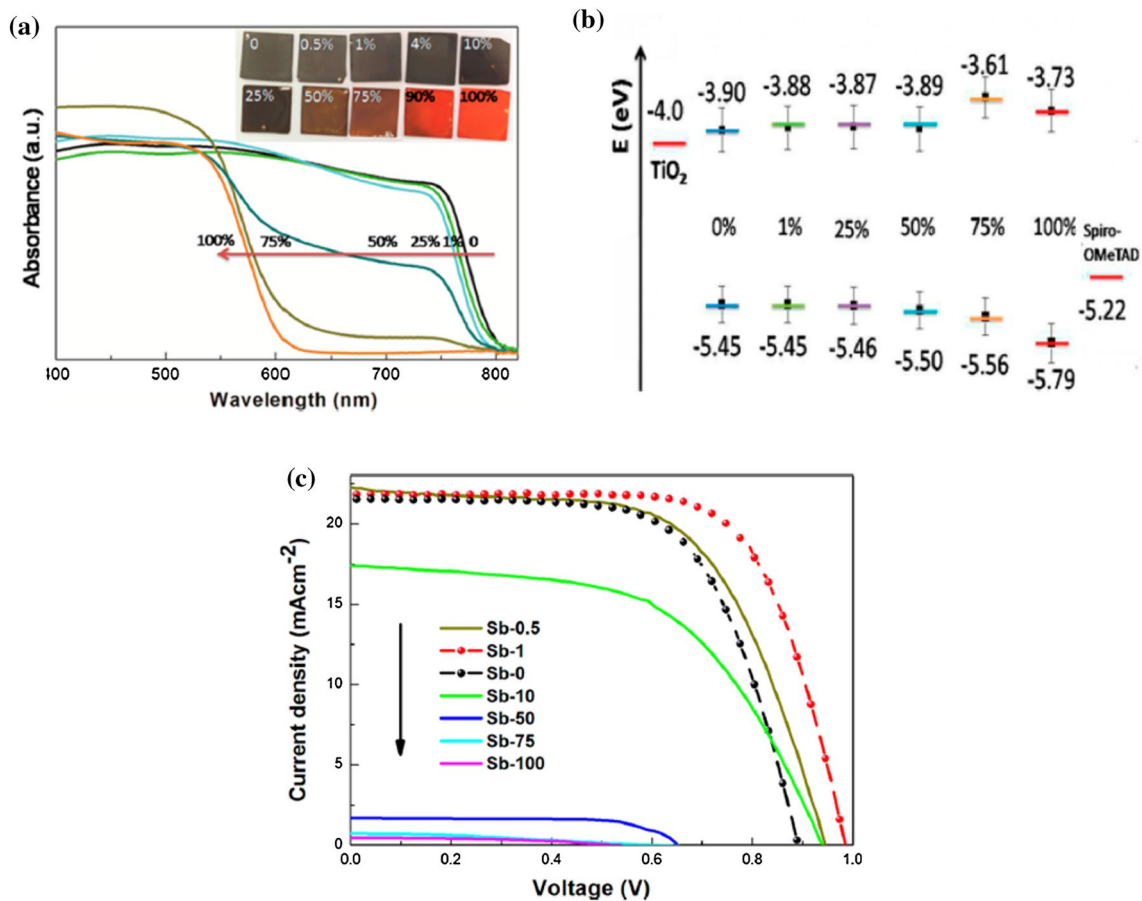


**Fig. 7** MAPb<sub>1-x</sub>Sb<sub>2x/3</sub>I<sub>3</sub> film properties: **a** UV–visible absorption spectra; **b** Estimated energy level diagram in vacuum; and **c** J–V curves. Reproduced with permission Copyright 2016, American Chemical Society

concentrations and post-deposition annealing temperatures. A Zn-doped perovskite layer resulted in perovskite absorbers with a larger grain size. Smooth films with large grain size inhibit the formation of pinholes and result in lower series resistance. With increasing Zn content, the number of pinholes increased significantly. The photoluminescence (PL) of the device also showed a significant increase as the Zn content increased (Fig. 8d, e). The allocation of Zn in the crystal structure reduced band edge interstate defects and thus increased carrier mobility and the lifetime of charge carriers.

## 2.6 Partial Substitution of Pb by Co, Cu, Fe, Mg, Mn, Ni, Sn, and Sr

A thorough investigation of the partial substitution of divalent metal species for Pb was carried out recently by Henry J. Snaith's group [57] using the composition MA(Pb:B\*)I<sub>3</sub>, where B\* = Co, Cu, Fe, Mg, Mn, Ni, Sn, Sr, and Zn. A screening study was conducted where 1.5–25% of the Pb was replaced with each element mentioned above, using

MAPbI<sub>3</sub> as a controlled material to understand the effect of partial replacement in PSCs. The PSCs fabricated in ITO/PEDOT:PSS/MA(Pb:B\*)I<sub>3</sub>/PCBM/BCP/Al configuration showed minimal hysteresis effect [58, 59]. Instead of using conventional precursor solution in the form of MAI:PbI [60, 61], divalent metal acetates, B\*(OAc)<sub>2</sub>, were chosen as metal precursors, since acetate salts are easily dissolved in DMF (except Ca and Sr). Lead acetate precursor also showed a similar capability to form high quality absorber film compared to conventional perovskite absorbers [62, 63]. Figure 9 shows the effect of partial substitution of MA(Pb:B\*)I<sub>3</sub> in terms of PCE. Amongst all the alternative elements, Fe shows detrimental device performance even at the smallest amount while Co produces the highest PCE.

Lower levels of Co partial substitution in PSCs were investigated and optimized due to their potential positive impact. Surface SEM images of the films (Fig. 10b–d) display changes of crystal structure as Co was included in the perovskite absorber film. It was observed that compact MAPbI<sub>3</sub> based film can be obtained using Pb(OAc)<sub>2</sub> without any visible pinholes. The crystal size of the film

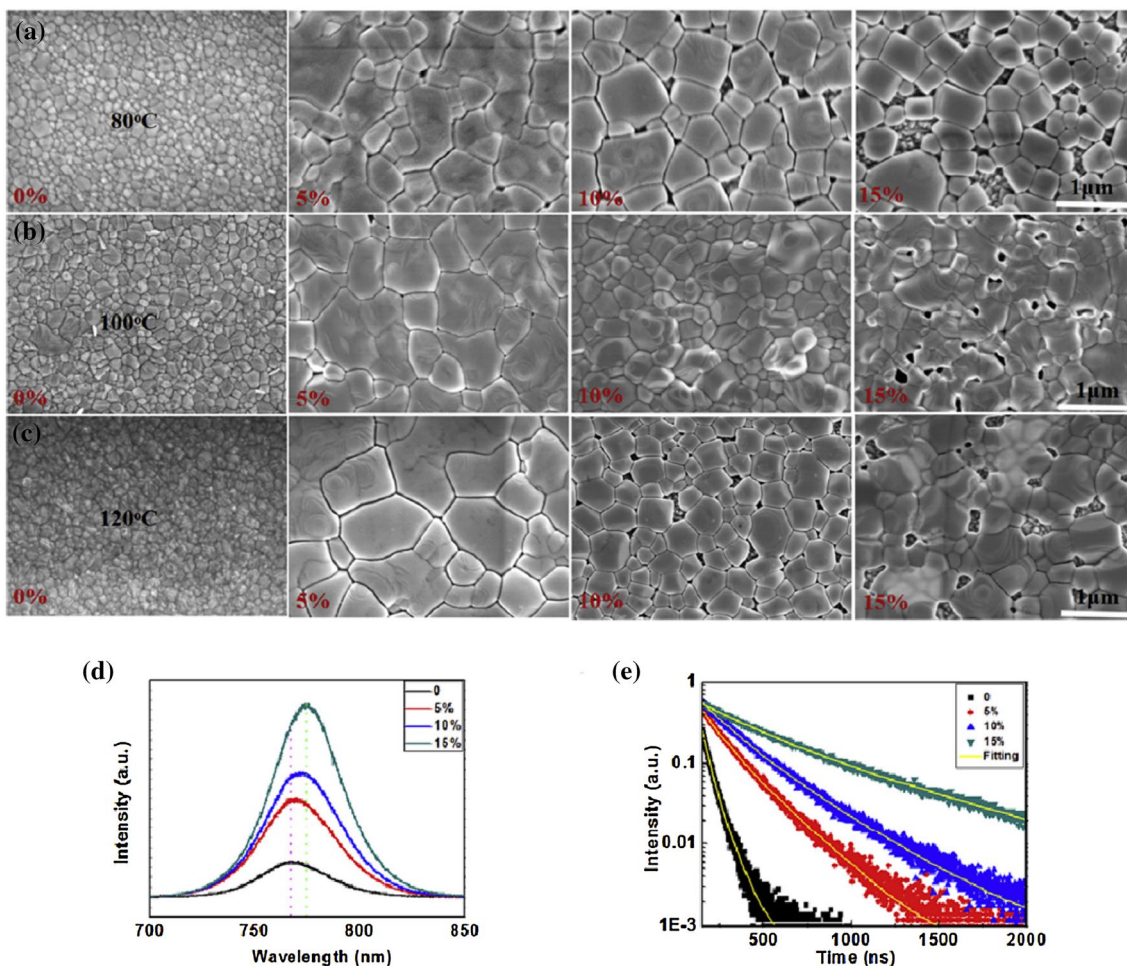


**Fig. 8** a–c FESEM images of various annealing temperatures of Zn-doped perovskite layer at 0, 5, 10, and 15% Zn; d PL spectra and e time-resolved photoluminescence spectroscopy. Reproduced with permission Copyright 2017, Elsevier

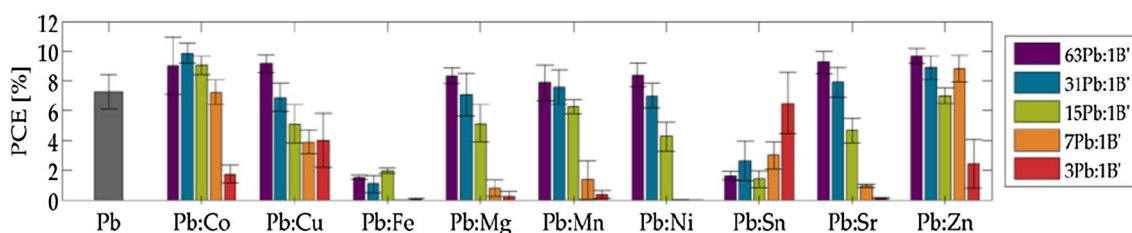


**Fig. 9** Average PCE of partially substituted (Co, Cu, Fe, Mg, Mn, Ni, Sn, Sr, and Zn) PSCs with pristine MAPbI<sub>3</sub> as control sample. Reproduced with permission [57] Copyright 2017, Royal Society of Chemistry

decreased as the amount of Co was increased and resulted in a compact pinhole-free layer. Lattice volume shrinkage by 0.86% indicates that Co successfully substituted for Pb inside the perovskite crystal structure, since the radius of Co<sup>2+</sup> is smaller than that of Pb<sup>2+</sup>. Interestingly, even when the amount of Co incorporation was varied at 63Pb:1Co, 31Pb:1Co, 15Pb:1Co, and 7Pb:1Co (Fig. 10e), the bandgap

of the device remained at 1.56 eV, which is similar to that of pristine MAPbI<sub>3</sub> film but differs from well-known Sn-incorporated PSCs [29, 33]. Partial incorporation of Co inside the perovskite crystal structure shifted the film band edge while maintaining the bandgap at 1.56 eV. However, insignificant change was observed between the Fermi level and the valence band edge (VBE). This discovery leads to

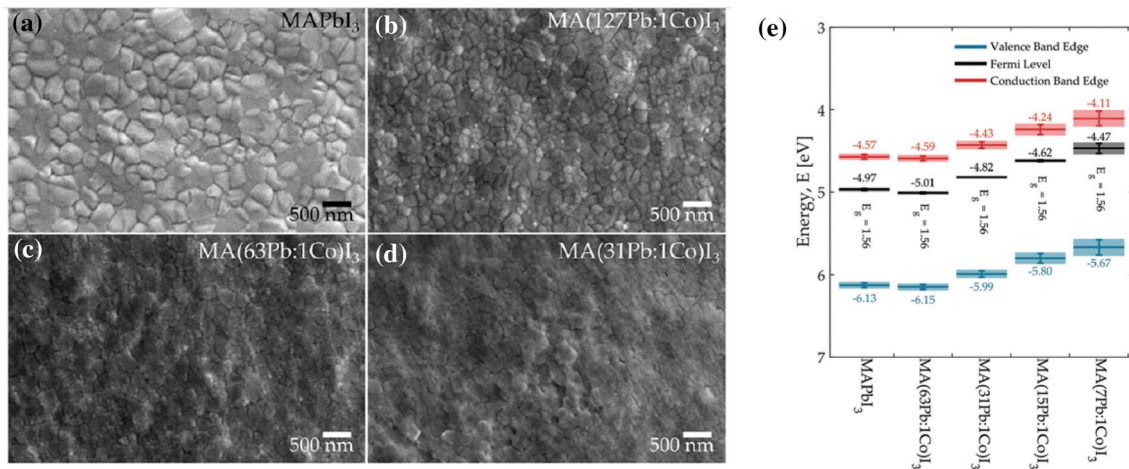


**Fig. 10** Surface SEM images for **a** MAPbI<sub>3</sub>, **b** MA(127Pb:1Co)I<sub>3</sub>, **c** MA(63Pb:1Co)I<sub>3</sub>, **d** MA(31Pb:1Co)I<sub>3</sub>, and energy levels of MA(Pb:Co)I<sub>3</sub> composition in vacuum determined by ultraviolet pho-

toelectron spectroscopy. Reproduced with permission [57] Copyright 2017, Royal Society of Chemistry

the possibility to tailor the work function of the film, thus a suitable alignment of bandgap between the absorber layer and subsequent charge carrier layers can be chosen to promote a better flow of charge carriers along the devices. If the Co<sup>2+</sup> fraction is limited to 0.8–1.6%, the J<sub>SC</sub> of the corresponding PSCs remains at the same level as that of

pristine MAPbI<sub>3</sub> based PSC. However, 3.1% Co<sup>2+</sup> fraction was found to be the tolerance limit of the PSC. The J<sub>SC</sub> value of the PSC displayed a sharp decrease when the composition was MA(31Pb:1Co)I<sub>3</sub> and MA(15Pb:1Co)I<sub>3</sub>. The V<sub>OC</sub> value increased steadily from a mean value of 0.96 V to 1.08 V as the amount of Co<sup>2+</sup> decreased. MA(63Pb:1Co)

**Table 1** List of reported partially substituted perovskite solar cells with their photovoltaic properties

Perovskite type	J <sub>SC</sub> (mA·cm <sup>-2</sup> )	V <sub>OC</sub> (V)	FF	Efficiency (%)	References
MAPb <sub>1-x</sub> Sn <sub>x</sub> I <sub>3</sub>	15.82	0.728	0.64	7.37	[31]
MAPb <sub>1-x</sub> Sn <sub>x</sub> I <sub>3</sub>	20.04	0.42	0.5	4.18	[28]
MAPb <sub>1-x</sub> Sn <sub>x</sub> I <sub>3</sub>	19.1	0.76	0.66	9.77	[33]
MAPb <sub>1-x</sub> Sr <sub>x</sub> I <sub>3</sub>	18	0.95	0.85	15	[54]
MAPb <sub>1-x</sub> Sn <sub>x</sub> I <sub>3</sub>	19	0.78	0.67	9.95	[64]
MAPb <sub>1-x</sub> Sn <sub>x</sub> I <sub>3</sub>	24.35	0.347	0.515	4.35	[26]
(FASnI <sub>3</sub> ) <sub>1-x</sub> (MAPbI <sub>3</sub> ) <sub>x</sub>	26.82	0.799	0.7	15	[23]
MAPb <sub>1-x</sub> Sn <sub>x</sub> I <sub>3-y</sub> Br <sub>y</sub>	15.52	1.04	0.78	12.59	[40]
MA <sub>1-x</sub> FA <sub>x</sub> Pb <sub>1-y</sub> Sn <sub>y</sub> I <sub>3</sub>	23.03	0.78	0.79	14.19	[65]
MAPb <sub>3-x</sub> Hg <sub>x</sub> I <sub>3</sub>	18.1	0.94	0.764	13	[50]
MA <sub>1-x</sub> Cs <sub>x</sub> Pb <sub>1-y</sub> Sn <sub>y</sub> I <sub>3</sub>	22.8	0.84	0.76	14.55	[66]
MAPb <sub>1-x</sub> Sn <sub>x</sub> I <sub>3</sub>	23.8	0.745	0.785	13.93	[67]
MAPb <sub>1-x</sub> In <sub>x</sub> I <sub>3</sub>	21.9	1.03	0.78	17.55	[24]
MAPb <sub>1-x</sub> Sn <sub>x</sub> I <sub>3</sub>	26.3	0.75	0.688	13.6	[68]
MAPb <sub>1-x</sub> Sb <sub>2x/3</sub> I <sub>3</sub>	21.82	0.985	0.692	15.6	[27]
MAPb <sub>1-x</sub> Ag <sub>x</sub> I <sub>3</sub>	20.6	1.10	0.81	18.4	[69]
MAPb <sub>1-x</sub> Co <sub>x</sub> I <sub>3</sub>	21.1	1.05	0.777	17.2	[57]
MAPb <sub>1-x</sub> Zn <sub>x</sub> I <sub>3</sub>	22.6	1.10	0.730	18.18	[56]
MAPb <sub>1-x</sub> Ge <sub>x</sub> I <sub>3</sub>	7.72	0.822	0.468	2.97	[70]
MAPb <sub>1-x</sub> Ti <sub>x</sub> I <sub>3</sub>	5.76	0.740	0.591	2.52	[70]
MAPb <sub>1-x</sub> In <sub>x</sub> I <sub>3</sub>	11.1	0.815	0.411	3.72	[70]
MAPb <sub>1-x</sub> As <sub>x</sub> I <sub>3+x</sub> Cl <sub>y</sub>	13.5	0.752	0.547	5.26	[71]
MAPb <sub>1-x</sub> Sb <sub>x</sub> I <sub>3-y</sub> Br <sub>y</sub>	12.8	0.774	0.653	6.47	[72]

I<sub>3</sub> was the highest performance device, which exceeded the performance of the pristine MAPbI<sub>3</sub> device.

Table 1 summarizes the overall photovoltaic performance of PSCs fabricated with partially substituted perovskite layers. The partially substituted Pb-based PSCs are comparatively stable in comparison to pure Pb-based PSCs. In terms of morphological impacts, partial substitution of Pb with other suitable elements results in better perovskite films and tend to result in higher efficiency PSCs. Controlling the type of cation and the percentage of alternative element inclusion provides tunable bandgap perovskite layers for PSCs. The unusual tunable optical properties of partially substituted Sn-based absorber has shown beneficial impact for tandem solar cell technology whether as a low (top) bandgap or a large (bottom) bandgap cell [73]. The small number of reports regarding partially substituted PSCs (excluding those with Sn) suggests there is narrow scope for other materials. However, it is critical to evaluate the suitability of each substituted element to obtain efficient PSC devices. Recent studies of partially substituted perovskite films imply that PSCs using Sr, Sb, Zn, Co, Hg, or In display significant improvements in device performance without sacrificing device stability. For further development of partially substituted perovskites towards commercialization, however, detailed research needs to be conducted.

### 3 Fully Substituted Perovskite Solar Cells

The development of new PSCs has been continuous since their first discovery and their scope has been widened considerably. Numerous studies have been conducted on incorporating impurities into conventional MAPbI<sub>3</sub> absorbers for increased carrier mobility [35], stability [53] and homogeneous crystallization [74]. Cation replacement of methylammonium iodide (CH<sub>3</sub>NH<sub>3</sub><sup>+</sup> (MA)) with cesium [75], formamidinium [21] and rubidium [76] has been successfully evaluated. Alternative halides to iodides such as Br [77] and Cl [78] have also been introduced within the absorber layer.

#### 3.1 Fully Substituted Sn-Based PSCs

Replacements of the Pb<sup>2+</sup> ion with similar elements have been pursued. As Sn is the major candidate for Pb replacement, Sn-based PSCs dominate the field of lead-free PSCs. Successful substitution of the Pb<sup>2+</sup> cation with the Sn<sup>2+</sup> cation achieved 6.4% PCE in the early years of PSC research [12] employing a mesoporous structure. In this pioneering work with CH<sub>3</sub>NH<sub>3</sub>SnI<sub>3</sub>, the perovskite crystals did not require heat treatment and successful absorber was formed naturally at room temperature. MASnI<sub>3</sub> crystals possess significant crystal defects due to spontaneous crystal formation. The absorption of MASnI<sub>3</sub> is higher than

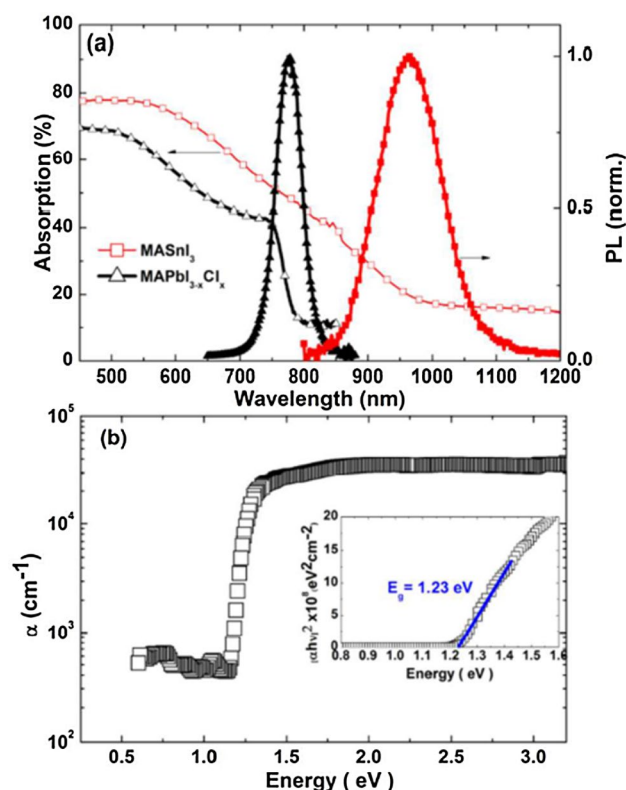


**Fig. 11** a Absorption and Photoluminescence of CH<sub>3</sub>NH<sub>3</sub>SnI<sub>3</sub> and CH<sub>3</sub>NH<sub>3</sub>PbI<sub>3-x</sub>Cl<sub>x</sub> crystals. b Tauc plot interpreted from absorption profile of CH<sub>3</sub>NH<sub>3</sub>SnI<sub>3</sub> crystals. Reproduced with permission [12] Copyright 2014, Royal Society of Chemistry

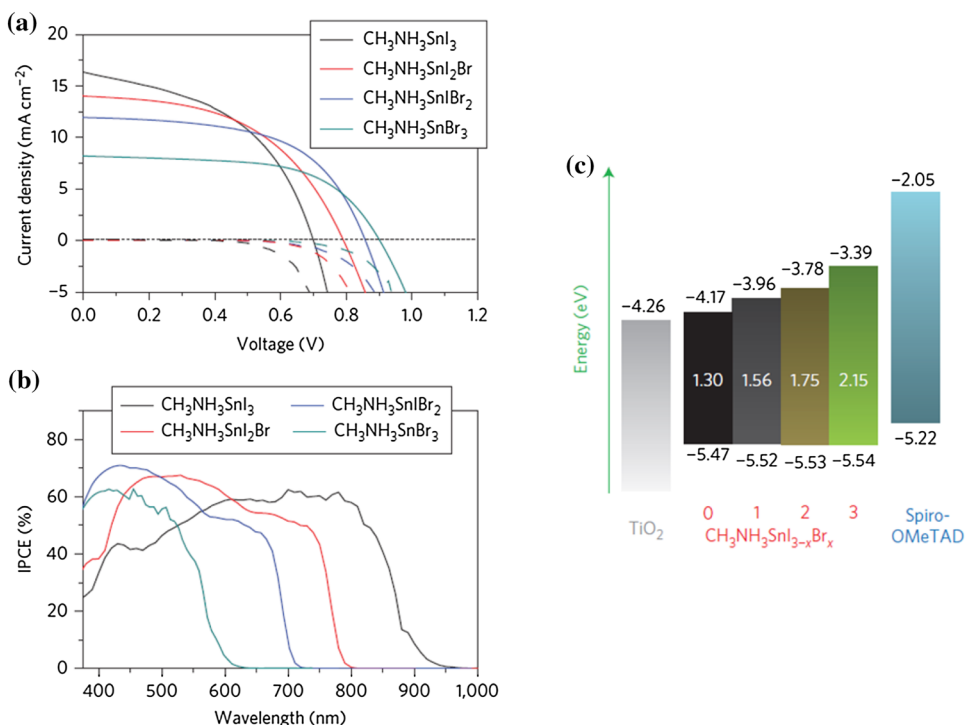
that of MAPbI<sub>3-x</sub>Cl<sub>x</sub>, which indicates better compatibility (Fig. 11a). In comparison to MAPbI<sub>3-x</sub>Cl<sub>x</sub> crystals, the photoluminescence peaks show wider absorption in the near infrared (NIR) zone. The MASnI<sub>3</sub> absorber also exhibits inferior photovoltaic properties compared to MAPbI<sub>3-x</sub>Cl<sub>x</sub> due to a low bandgap of 1.23 eV (Fig. 11b) compared to the MAPbI<sub>3</sub> absorber (1.55 eV). This lower bandgap affects band alignment between the absorber and the corresponding charge extraction layer. Sn<sup>2+</sup> is easily converted to Sn<sup>4+</sup> in air, which leads to substandard performance as its photovoltaic properties are reduced [30].

A Sn-based mesoporous PSC mixed halide absorber with 5.73% PCE was reported by Kanatzidis et al. [79]. Inclusion of bromide with iodide (Fig. 12a) increased the open-circuit voltage (V<sub>OC</sub>) but reduced the current density (J<sub>SC</sub>) in the corresponding PSC. The variation of J<sub>SC</sub> correlates with the IPCE spectra of MASnI<sub>3-x</sub>Br<sub>x</sub>-based PSCs with varying amounts of Br inclusion (600–950 nm) (Fig. 12b). V<sub>OC</sub> values of 1.30, 1.56, 1.7, and 2.15 eV are attributed to changes in the CH<sub>3</sub>NH<sub>3</sub>SnI<sub>3-x</sub>Br<sub>x</sub> bandgap where x = 0, 1, 2, and 3, respectively (Fig. 12c).

Early studies of Sn-based perovskites suffered from spontaneous oxidation of Sn<sup>2+</sup> to Sn<sup>4+</sup> [12, 79]. Gratzel



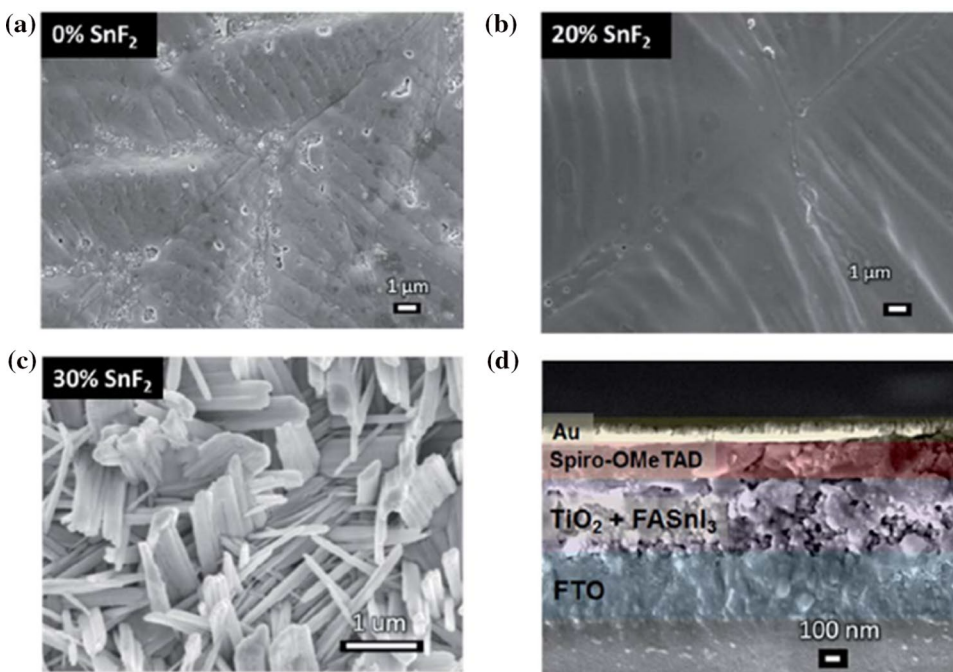
**Fig. 12** Characteristics of  $\text{MASnI}_{3-x}\text{Br}_x$  **a** J-V curve, **b** IPCE Spectra, **c** Energy Level diagram. Reproduced with permission [79] Copyright 2016, Nature Publishing Group



et al. reported Pb-free PSC using Cs as the cation to substitute the MA cation [20]. The addition of  $\text{SnF}_2$  into the  $\text{CsSnI}_3$  managed to suppress the involuntary oxidation of  $\text{Sn}^{2+}$  to  $\text{Sn}^{4+}$  by occupying the intrinsic defects, resulting in metallic properties. Mathew et al. reported on the usage of  $\text{HC}(\text{NH}_2)_2\text{PbI}_3$  (FASnI<sub>3</sub>) as the absorber in a mesoporous PSC [37]. With the addition of  $\text{SnF}_2$ , reduced degradation

of the  $\text{HC}(\text{NH}_2)_2\text{PbI}_3$  (FASnI<sub>3</sub>) absorber has been observed. Inclusion of 20%  $\text{SnF}_2$  (optimum amount) into the film resulted in homogenous crystallization throughout the absorber (Fig. 13b). Aggregation of the crystals formed nanoplatelets with an excess amount of  $\text{SnF}_2$  added. Inclusion of 30%  $\text{SnF}_2$  increased the film roughness due to induced phase separation (Fig. 13c). The usage of Dimethylformamide

**Fig. 13** FESEM image (top) view for FASnI<sub>3</sub> with different amounts of  $\text{SnF}_2$  **a** 0%  $\text{SnF}_2$  **b** 20%  $\text{SnF}_2$ ; and **c** Cross-sectional FESEM view for full FASnI<sub>3</sub> mesoporous PSC. Reproduced with permission [37] Copyright 2015, Royal Society of Chemistry



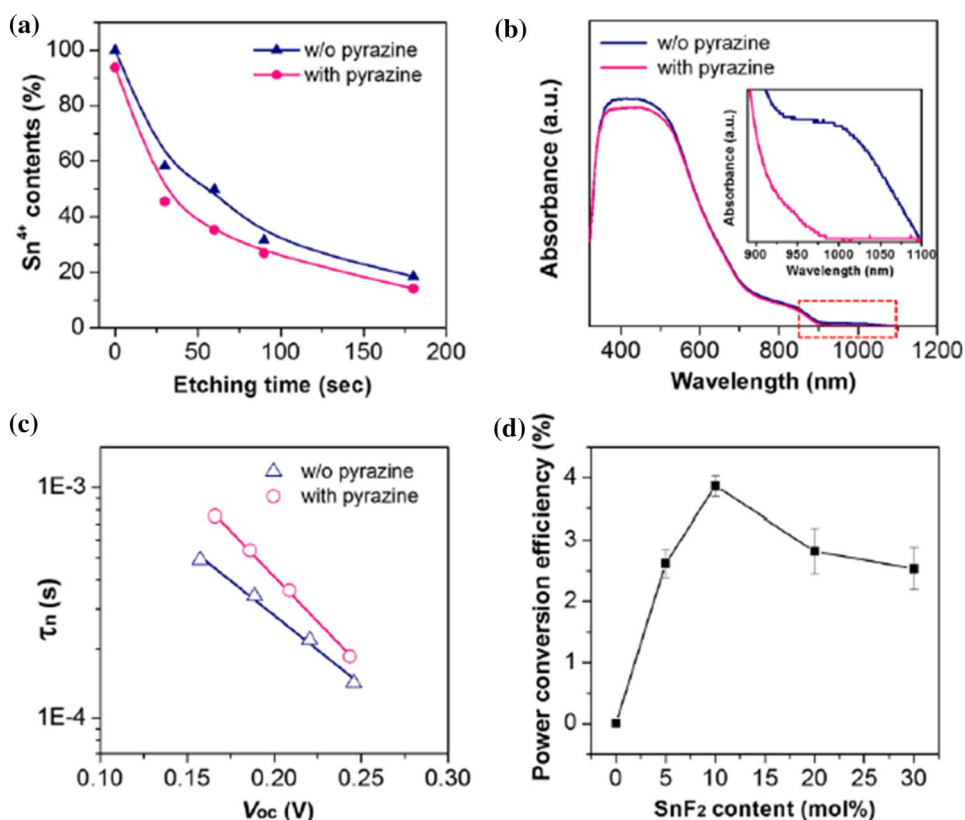
(DMF), Dimethyl sulfoxide (DMSO), gamma-Butyrolactone (GBL), and N-Methyl-2-pyrrolidone (NMP) have gained popularity for MAPbI<sub>3</sub> film deposition in PSCs [7, 80, 81]. Successful formation of MAPbI<sub>3</sub> films has been observed with post-annealing treatment at 100 °C. In contrast, a novel deposition method using an appropriate solvent for MASnI<sub>3</sub> film was introduced by Kanatzidis et al. [22]. Intermediate phases were observed with coordination of DMSO and MAPbI<sub>3</sub> [82]. It was noticed that MASnI<sub>3</sub> crystallizes rapidly from DMF solvent during spin coating but as DMF was swapped with DMSO, the film did not spontaneously convert to black but changed to light yellow instead. This could be due to the formation of an MAPbI<sub>3</sub>.DMSO intermediate complex. Nonetheless, the complex form was identified as a SnI<sub>3</sub>.3DMSO intermediate which suppressed premature crystallization. Subsequent heat treatment (100 °C) fully converted the intermediate to a dense, pinhole-free film with inclusion of a 10% SnF<sub>2</sub> additive.

Sang Il Seok's group reported enhanced performance of FASnI<sub>3</sub>-based PSC with superior efficiency and stability [36]. The addition of pyrazine resulted in bonding with SnF<sub>2</sub> and successfully prevented phase separation. The low boiling point of pyrazine (115 °C) also resulted in easy annealing of the FASnI<sub>3</sub> absorber. The addition of SnF<sub>2</sub> strongly influences its role of suppressing Sn<sup>4+</sup> formation when included (Fig. 14a). Since the absorption onset for FASnI<sub>3</sub> is reduced from 1100 nm to 1000 nm by adding pyrazine, the crystal

structure is likely more stable (Fig. 14b). This phenomenon decreased the recombination time with increasing V<sub>OC</sub>. The best PCE was observed with 10 mol % of SnF<sub>2</sub> content (Fig. 14d). The FA cation also proved to significantly reduce degradation as FA-based Sn-based complexes were more stable than MA-based ones [37]. Additionally, FA-based Sn perovskites have a wider bandgap of ~1.4 eV [83].

The fabricated device easily reached a maximum of 4.8% PCE with a high value of J<sub>SC</sub> (23.7 mAcm<sup>-2</sup>) but a low value of V<sub>OC</sub> (0.32 V). The major step between the CBM of FASnI<sub>3</sub> (3.3 eV) and TiO<sub>2</sub> (~4.2 eV) resulted in the low V<sub>OC</sub> value [25, 84]. However, the PSC maintained 98% of its initial efficiency after 100 days with encapsulation. Due to an unprecedented loss of V<sub>OC</sub> in the Sn-based mesoporous PSCs, Kanatzidis et al. [84] introduced a thin layer of ZnS between the mesoporous TiO<sub>2</sub> and FASnI<sub>3</sub>. Inclusion of this thin interfacial ZnS layer formed a cascade, inducing movement of electrons towards the mesoporous TiO<sub>2</sub> layer and extracted to the load instead of recombining inside the corresponding PSC. The ZnS interfacial layer efficiently blocked any electron backflow and recombined with holes in the VBM at the FASnI<sub>3</sub> layer. Without ZnS, the difference between TiO<sub>2</sub> CBM and FASnI<sub>3</sub> VBM was only ~0.5 eV which led to promotion of electron backflow, resulting in a lower V<sub>OC</sub> value. The V<sub>OC</sub> of TiO<sub>2</sub>/ZnS based PSC increased from 0.29 V for bare TiO<sub>2</sub> to 0.37 V. The device also showed a better quenching effect in PL due to a

**Fig. 14** **a** Sn<sup>4+</sup> content calculated from X-ray photoelectron spectroscopy (XPS) inside the FASnI<sub>3</sub> absorber; **b** absorbance of FASnI<sub>3</sub> with and without pyrazine addition; **c** recombination time of FASnI<sub>3</sub> absorber with and without pyrazine addition; **d** correlation between SnF<sub>2</sub> content and power conversion efficiency (PCE). Reproduced with permission [36] Copyright 2016, American Chemical Society



better electron transfer process stimulated by ZnS incorporation. Time-resolved photoluminescence (TRPL) showed faster transition of electrons between the layers at 0.85 ns ( $\text{TiO}_2 = 2.52$  ns). The best cell for this structure showed a PCE of 5.27% with  $V_{\text{OC}} = 0.380$  V,  $J_{\text{SC}} = 23.09$   $\text{mA}\cdot\text{cm}^{-2}$ , and  $\text{FF} = 0.6$ . According to a previous optimal bandgap alignment study [85–87] for other types of solar cells, choosing suitable material/structure for Sn-based cells played a crucial role in developing higher performance devices. Yanfa Yan et al. reported an inverted planar structure  $\text{FASnI}_3$ -based PSC with an efficiency exceeding 6% [25]. With DMSO as the  $\text{FASnI}_3$  precursor solvent, the  $\text{FASnI}_3$  based PSC was fabricated as an ITO/PEDOT: PSS/ $\text{FASnI}_3$ /Fullerene/BCP/Ag configuration. This work resulted in  $V_{\text{OC}} = 0.465$  V,  $J_{\text{SC}} = 22.07$   $\text{mA}\cdot\text{cm}^{-2}$ , and  $\text{FF} = 0.606$  in reverse scan. The preferred band alignment in the inverted PSC led to better electron migration as the energy barrier in the mesoporous PSC structure was successfully avoided. For deposition of  $\text{FASnI}_3$ , diethyl ether was used as the dripping solvent instead of toluene or chlorobenzene. Dense uniform  $\text{FASnI}_3$  film with a high stability maintaining 90% of its initial efficiency was obtained when  $\text{SnF}_2$  additive was included in the film. Although Sn-based PSCs have been intensely investigated, they have failed to attain a high PCE exceeding 10%. Chienyi Chen et al. reported a PCE of 12.96% in a PSC comprised of  $\text{CsSnX}$  ( $X = \text{Cl}, \text{Br}, \text{I}$ ) as the perovskite absorber [88]. Fabricated  $\text{CsSnX}$  ( $X = \text{Cl}, \text{Br}, \text{I}$ ) quantum rods (QR) were incorporated in a mesoporous structure with photovoltaic parameters of  $J_{\text{SC}} = 23.21$   $\text{mA}\cdot\text{cm}^{-2}$ ,  $V_{\text{OC}} = 0.86$  V, and  $\text{FF} = 0.65$  for  $\text{CsSnI}_3$  absorber. The  $\text{CsSnI}_3$  QRs were fabricated through a solvothermal process and displayed excellent optical properties. The iodine-based  $\text{CsSnX}$  perovskite absorbers showed better photovoltaic properties compared to the other two halides. The solvothermal process is widely known as a common bottom-up method for

fabricating nanoparticles [89–91]. The solvothermal process also provides homogenous nucleation, as demonstrated by Energy Dispersion Spectroscopy (EDS) elemental mapping images (Fig. 15) of  $\text{CsSnI}_3$  QR showing an even distribution of Cs, Sn, and I elements at a 1:1:3 ratio. The process also allows homogenous formation of the QR during the insignificant defect contrast in PL emission.  $\text{CsSnI}_3$  QR exhibited less intrinsic defects than Cl/Br-based ones, as the full width half maxima (FWHM) PL emissions are narrower than for the other two halides.

The  $\text{CsSnX}$  absorber film preparation demonstrated successful dispersion of QR on top of mesoporous  $\text{TiO}_2$ . The prepared QRs were dispersed in toluene and spin-coated on top of mesoporous  $\text{TiO}_2$  for preparation of Sn-Based PSC. This example shows that inorganic ions such as Cs can replace popular cations such as MA or FA [80, 81]. Superior photovoltaic traits of the QRs were shown by its ability to reach a  $J_{\text{sc}}$  value of up to 23  $\text{mA}\cdot\text{cm}^{-2}$  (Fig. 16a, b). As the halides were substituted from I to Br to Cl, the PCE decreased in that order. This can be explained by the bandgaps for I, Br, and Cl as they vary with the absorption onset wavelength reducing from 709 nm ( $\sim 1.7$  eV) to 668 nm ( $\sim 1.85$  eV) to 588 nm ( $\sim 2.1$  eV), respectively. The Cs cation influenced the performance and thermal stability of the fabricated PSC compared to the MA cation and the efficiency retained after 16 days under an oxygen atmosphere was higher than for  $\text{MAPbI}_3$  (Fig. 16c).

### 3.2 Alternate Perovskite Compounds

As described in the previous sections, substitution of Pb with Sn in perovskite can produce promising results. However, due to its inferior photovoltaic performance with minimal stability, other alternatives to Sn are under constant investigation. Bismuth was introduced by Park's

**Fig. 15** a High-resolution TEM images of  $\text{CsSnI}_3$  QR b TEM image of obtained  $\text{CsSnI}_3$  QR with respective energy dispersion spectroscopy (EDS) elemental image mapping for elements: c Cs, d Sn, and e I. Reproduced with permission [88] Copyright 2016, American Chemical Society

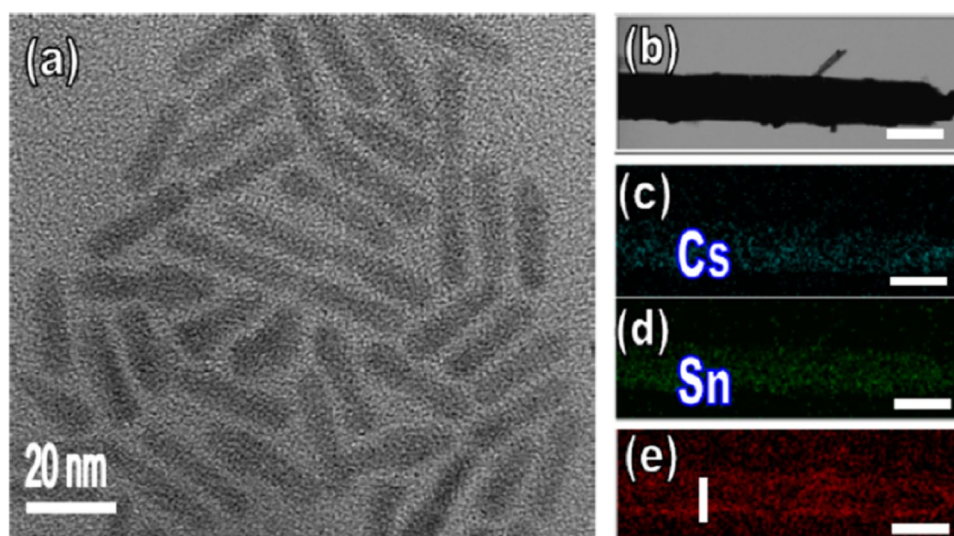
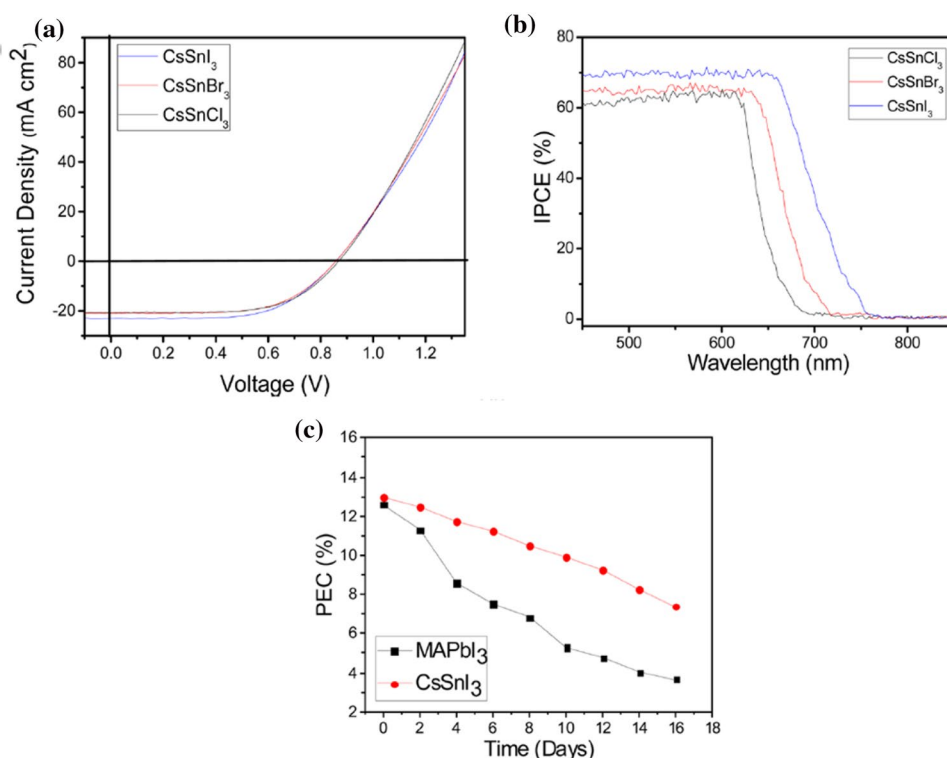


**Fig. 16** **a** J-V curve and **b** EQE of CsSnI<sub>3</sub> (blue), CsSnBr<sub>3</sub> (red), and CsSnCl<sub>3</sub> (black). **c** Efficiency degradation comparison between MAPbI<sub>3</sub> and CsSnI<sub>3</sub> based. Reproduced with permission [88] Copyright 2016, American Chemical Society. (Color figure online)



group in multiple compositions (e.g. Cs<sub>3</sub>Bi<sub>2</sub>I<sub>9</sub>, MA<sub>3</sub>Bi<sub>2</sub>I<sub>9</sub>, MA<sub>3</sub>Bi<sub>2</sub>I<sub>9</sub>Cl<sub>x</sub>) but showed only ~1% efficiency [13]. In an exploration of new substitute elements, the strain required to form a homogenous uniform perovskite layer has been identified as a crucial issue. The inevitable formation of defect density forms trap states around the corresponding absorber layer, limiting the overall photovoltaic response (Fig. 17a). Figure 17b shows J-V curves of PSCs fabricated with Cs<sub>3</sub>Bi<sub>2</sub>I<sub>9</sub>, MA<sub>3</sub>Bi<sub>2</sub>I<sub>9</sub>, and MA<sub>3</sub>Bi<sub>2</sub>I<sub>9</sub>Cl<sub>x</sub>. The absorption coefficient of Bi-based perovskite absorber ( $1 \times 10^5 \text{ cm}^{-1}$ ) was identified as lower than that of Pb-based perovskite absorber ( $2 \times 10^5 \text{ cm}^{-1}$ ) with a similar thickness of 450 nm [92].

The bandgaps for Cs<sub>3</sub>Bi<sub>2</sub>I<sub>9</sub>, MA<sub>3</sub>Bi<sub>2</sub>I<sub>9</sub>, and MA<sub>3</sub>Bi<sub>2</sub>I<sub>9</sub>Cl<sub>x</sub> films were observed around 2.2, 2.1 and 2.4 eV, respectively. The theoretical PCE for absorbers with 2 eV of 20% has been determined by the Shockley–Queisser limit [93]. Figure 17c depicts the PL spectra where it has been identified that non-radiative recombination occurs in MA<sub>3</sub>Bi<sub>2</sub>I<sub>9</sub> and MA<sub>3</sub>Bi<sub>2</sub>I<sub>9</sub>Cl<sub>x</sub> films while Cs<sub>3</sub>Bi<sub>2</sub>I<sub>9</sub> crystals show a luminescence response around 660 nm. The FWHM of the peak suggests the existence of numerous interstate bandgap defects. This early stage investigation elucidated the exact issue concerning the photovoltaic performance of Cs<sub>3</sub>Bi<sub>2</sub>I<sub>9</sub>, MA<sub>3</sub>Bi<sub>2</sub>I<sub>9</sub>, and MA<sub>3</sub>Bi<sub>2</sub>I<sub>9</sub>Cl<sub>x</sub> absorbers as the determining factor. Until now, only Cu [94], Sb<sup>15</sup>, and Ge<sup>14</sup> have been introduced as other alternate materials for substitution of Pb in PSCs.

As the major candidate for Pb replacement, Sn is under constant investigation for use in lead-free PSCs as shown in Table 2. The basic properties of Sn have been explored for many decades, which may provide a basis for further improvement of lead-free devices [105–107]. Although theoretical study provides better understanding of the nature of materials, the study of Sn-based perovskite absorbers for efficient PSCs still requires ideal conditions, which are not relevant to real-world conditions. Therefore, the study of alternative materials as a replacement to Pb is still hindered, although progress with Sn-based PSCs is headed in the right direction. Intensive investigations into material properties are still greatly needed in order for new upcoming materials to challenge Sn-based PSCs. Despite good efforts to fully substitute Pb in PSCs, the highest efficiency achieved for lead-free devices is below 7% PCE, falling short of what has been achieved with Pb-based PSCs.

## 4 Conclusions

Development of PSCs containing low-toxicity elements for replacement of Pb in conventional PSCs has been reviewed in this article. Theoretical studies according to blackbody thermodynamic limits have shown that the PCE of Sn-based PSCs (1.34 eV) can be as high as 34% whereas the PCE of Pb-based PSCs (1.48 eV) falls short by 2% (32%). This demonstrates that Sn-based PSCs are still in their early phase



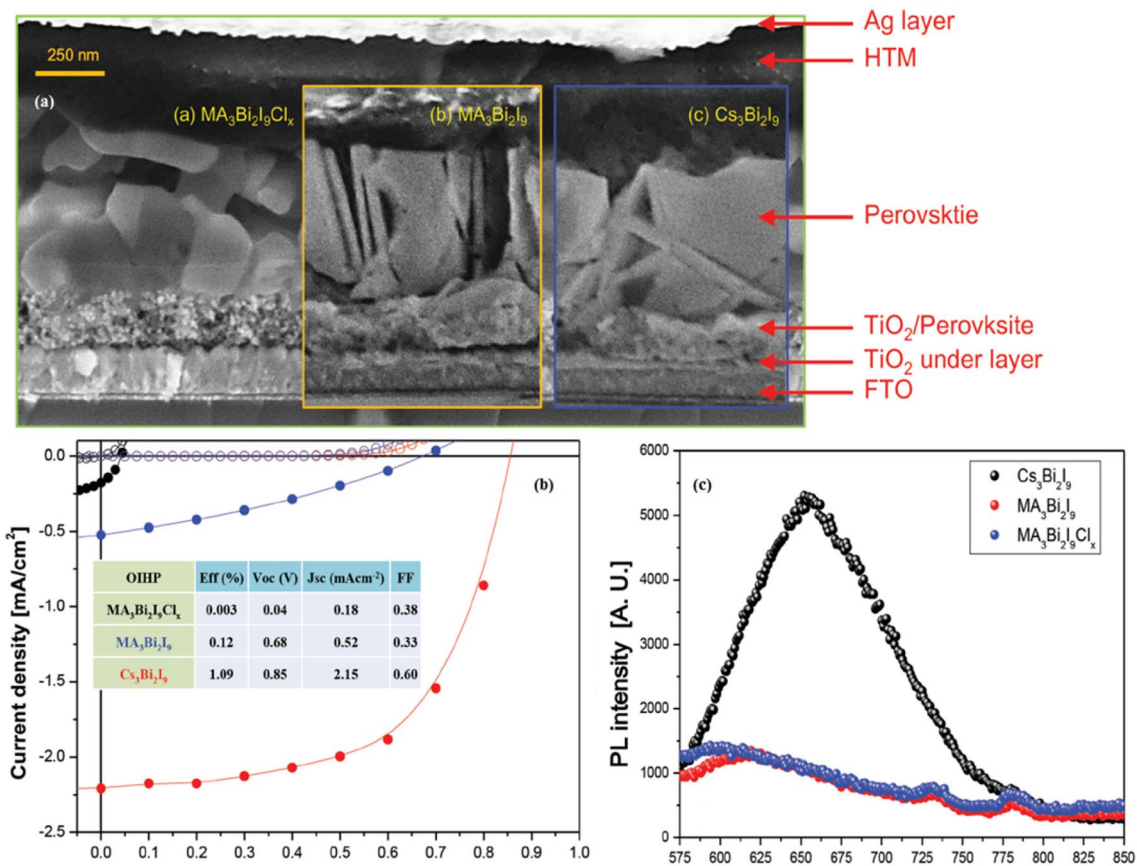


**Fig. 17** **a** Cross-sectional SEM images of Cs<sub>3</sub>Bi<sub>2</sub>I<sub>9</sub>, MA<sub>3</sub>Bi<sub>2</sub>I<sub>9</sub>, and MA<sub>3</sub>Bi<sub>2</sub>I<sub>9</sub>Cl<sub>x</sub> PSCs; **b** J-V curves of PSCs fabricated with Cs<sub>3</sub>Bi<sub>2</sub>I<sub>9</sub>, MA<sub>3</sub>Bi<sub>2</sub>I<sub>9</sub>, and MA<sub>3</sub>Bi<sub>2</sub>I<sub>9</sub>Cl<sub>x</sub>; **c** PL Spectra of Cs<sub>3</sub>Bi<sub>2</sub>I<sub>9</sub>, MA<sub>3</sub>Bi<sub>2</sub>I<sub>9</sub>,

and MA<sub>3</sub>Bi<sub>2</sub>I<sub>9</sub>Cl<sub>x</sub> films. Reproduced with permission [13] Copyright 2015 John Wiley & Sons

of research in terms of the photovoltaic response obtained so far. Introduced pristine Sn-based films are still unable to contain the crystal phase because phase separation occurs under ambient conditions, which eventually leads to degradation of the material (Sn<sup>2+</sup> to Sn<sup>4+</sup>). Addition of various compounds can inhibit phase separation in ambient air, allowing a significant reduction of this degradation. Part of the stability issue has been solved by inverted planar PSC structure utilization which avoids any salt requirement within the HTM. For assurance of fine film crystalline quality, DMSO solvent usage procures intermediate phases of Sn perovskite during post-annealing which are crucial in either Pb-based or Sn-based perovskites. High quality film prevents any unnecessary crystal defects with better photovoltaic performance. For alternative lead-free compounds, device performance is still much lower than that for Sn-based PSCs due to their unpredictable crystallization mechanics. Partially substituted Sn-based film is useful for

lowering toxicity with a broader absorption range up to the NIR zone. Higher amounts of Pb protect Sn<sup>2+</sup> inclusion in the structure by avoiding device degradation. But in certain cases, with precursor engineering, higher amounts of Sn substitute can result in high efficiency PSCs. The properties of partially substituted perovskite absorbers in corresponding PSCs reveal their suitability for inclusion in tandem solar cells, either for top or bottom cells. In partially substituted low-toxicity (excluding Sn) PSCs, a very small amount of univalent or trivalent substitute candidate assists in forming high quality film crystallization dynamics. The evolution pathways of low-toxicity PSCs show promise for a bright future for these materials. Further investigation on film formation and dynamics will enhance the compatibility of Sn-based PSCs for eventual industrial application. The ultimate dream of lead-free low-toxicity PSCs could be realized in the near future.

**Table 2** List of reported lead-free perovskites with their photovoltaic properties

Perovskite type	$J_{sc}$ (mA·cm <sup>-2</sup> )	$V_{oc}$ (V)	FF	Efficiency (%)	References
MASnI <sub>3</sub>	16.8	0.88	0.42	6.4	[12]
MASnI <sub>3-x</sub> Br <sub>x</sub>	12.3	0.82	0.57	5.73	[79]
MASnI <sub>3</sub>	15.18	0.716	0.5	5.44	[31]
CsSnI <sub>3</sub>	22.7	0.24	0.37	2.02	[20]
MASnI <sub>3</sub>	21.4	0.32	0.46	3.15	[79]
FASnI <sub>3</sub>	24.45	0.238	0.36	2.1	[37]
Cs <sub>3</sub> Bi <sub>2</sub> I <sub>9</sub>	2.15	0.85	0.6	1.09	[13]
MA <sub>3</sub> Bi <sub>2</sub> I <sub>9</sub>	0.52	0.68	0.33	0.12	[13]
MA <sub>3</sub> Bi <sub>2</sub> I <sub>9</sub> Cl	0.18	0.04	0.38	0.003	[13]
CsGeI <sub>3</sub>	5.7	0.074	0.27	0.11	[94]
MAGeI <sub>3</sub>	4	0.15	0.3	0.2	[94]
CsSnIBr <sub>2</sub>	24.16	0.222	0.33	1.76	[20]
HDABiI <sub>5</sub>	0.124	0.403	0.43	0.027	[95]
FASnI <sub>3</sub>	23.7	0.32	0.63	4.8	[36]
MASnI <sub>3</sub>	17.36	0.273	0.39	1.86	[96]
FASnI <sub>3-x</sub> Br <sub>x</sub>	6.82	0.467	0.54	1.72	[97]
CsSnI <sub>3</sub>	23.2	0.86	0.65	12.96	[88]
CsSnBr <sub>3</sub>	21.23	0.85	0.58	10.46	[88]
CsSnCl <sub>3</sub>	19.82	0.87	0.56	9.66	[88]
CsSnBr <sub>3</sub>	9.1	0.4	0.56	2.04	[98]
MaSnI <sub>3-x</sub> Br <sub>x</sub>	3.4	0.7	–	1.25	[99]
MASnI <sub>3</sub>	3.15	0.8	–	1.51	[99]
FASnI <sub>3</sub>	23.09	0.38	0.6	5.27	[84]
MASnI <sub>3</sub>	12.1	0.377	0.366	1.7	[100]
MASnBr <sub>3</sub>	4.27	0.498	0.491	1.12	[101]
MASnI <sub>3</sub>	19.92	0.377	0.518	3.89	[102]
CsSnI <sub>3</sub>	30.75	0.17	0.348	1.83	[102]
CsSnBr <sub>3</sub>	13.96	0.366	0.593	3.04	[102]
CsSnIBr <sub>2</sub>	16.7	0.33	0.53	3	[103]
FASnI <sub>3</sub>	22.07	0.457	0.60	6.07	[25]
MACuCl <sub>3-x</sub> Br <sub>x</sub>	0.216	0.256	0.32	0.017	[14]
Cs <sub>2</sub> SnI <sub>6</sub>	5.41	0.51	0.35	0.96	[104]

**Acknowledgements** Ashrafal Islam acknowledges support from JSPS KAKENHI Grant 18H02079. Ashrafal Islam and Jae-Joon Lee also acknowledge support from NRF-2016M1A2A2940912 and 2015M1A2A2054996. This work was partly supported by the Ministry of Higher Education (MOHE) Malaysia research grant with code-FRGS/1/2017/TK07/UKM/02/9. I. Bedja extends his appreciation to the Deanship of Scientific Research at King Saud University for funding this work through research group NO (RG-1438-041) and RSSU at King Saud University for their technical support.

## References

- Kojima, A., Teshima, K., Shirai, Y., Miyasaka, T.: Organometal halide perovskites as visible-light sensitizers for photovoltaic cells. *J. Am. Chem. Soc.* **131**, 6050–6051 (2009)
- Im, J.-H., Lee, C.-R., Lee, J.-W., Park, S.-W., Park, N.-G.: 6.5% efficient perovskite quantum-dot-sensitized solar cell. *Nanoscale* **3**, 4088–4093 (2011)
- Kim, H.-S., Lee, C.-R., Im, J.-H., Lee, K.-B., Moehl, T., Marchioro, A., Moon, S.-J., Humphry-Baker, R., Yum, J.-H., Moser, J.E.: Lead iodide perovskite sensitized all-solid-state submicron thin film mesoscopic solar cell with efficiency exceeding 9%. *Sci. Rep.* **2**, 591 (2012)
- Lee, M.M., Teuscher, J., Miyasaka, T., Murakami, T.N., Snaith, H.J.: Efficient hybrid solar cells based on meso-structured organometal halide perovskites. *Science* **338**, 643–647 (2012)
- Burschka, J., Pellet, N., Moon, S.-J., Humphry-Baker, R., Gao, P., Nazeeruddin, M.K., Grätzel, M.: Sequential deposition as a route to high-performance perovskite-sensitized solar cells. *Nature* **499**, 316–319 (2013)
- Chen, Q., Zhou, H., Hong, Z., Luo, S., Duan, H.-S., Wang, H.-H., Liu, Y., Li, G., Yang, Y.: Planar heterojunction perovskite solar cells via vapor-assisted solution process. *J. Am. Chem. Soc.* **136**, 622–625 (2013)
- Wu, Y., Islam, A., Yang, X., Qin, C., Liu, J., Zhang, K., Peng, W., Han, L.: Retarding the crystallization of PbI<sub>2</sub> for highly reproducible planar-structured perovskite solar cells via sequential deposition. *Energy Environ. Sci.* **7**, 2934–2938 (2014)


8. Son, D.-Y., Im, J.-H., Kim, H.-S., Park, N.-G.: 11% efficient perovskite solar cell based on ZnO nanorods: an effective charge collection system. *J. Phys. Chem. C* **118**, 16567–16573 (2014)
9. Eperon, G.E., Burlakov, V.M., Docampo, P., Goriely, A., Snaith, H.J.: Morphological control for high performance, solution-processed planar heterojunction perovskite solar cells. *Adv. Funct. Mater.* **24**, 151–157 (2014)
10. Kumar, M.H., Yantara, N., Dharani, S., Graetzel, M., Mhaisalkar, S., Boix, P.P., Mathews, N.: Flexible, low-temperature, solution processed ZnO-based perovskite solid state solar cells. *Chem. Commun.* **49**, 11089–11091 (2013)
11. Gilfillan, S.C.: Lead poisoning and the fall of Rome. *J. Occup. Environ. Med.* **7**, 53–60 (1965)
12. Noel, N.K., Stranks, S.D., Abate, A., Wehrenfennig, C., Guarnera, S., Haghighirad, A.-A., Sadhanala, A., Eperon, G.E., Pathak, S.K., Johnston, M.B.: Lead-free organic–inorganic tin halide perovskites for photovoltaic applications. *Energy Environ. Sci.* **7**, 3061–3068 (2014)
13. Park, B.W., Philippe, B., Zhang, X., Rensmo, H., Boschloo, G., Johansson, E.M.: Bismuth based hybrid perovskites  $A_3Bi_2I_9$  (A: methylammonium or cesium) for solar cell application. *Adv. Mater.* **27**, 6806–6813 (2015)
14. Cortecchia, D., Dewi, H.A., Yin, J., Bruno, A., Chen, S., Baikie, T., Boix, P.P., Grätzel, M., Mhaisalkar, S., Soci, C.: Lead-free  $MA_2CuCl_xBr_{4-x}$  hybrid perovskites. *Inorg. Chem.* **55**, 1044–1052 (2016)
15. Hebig, J.-C., Kühn, I., Flohre, J., Kirchartz, T.: Optoelectronic properties of  $(CH_3NH_3)_3Sb_2I_9$  thin films for photovoltaic applications. *ACS Energy Lett.* **1**, 309–314 (2016)
16. Chen, W., Wu, Y., Yue, Y., Liu, J., Zhang, W., Yang, X., Chen, H., Bi, E., Ashraful, I., Grätzel, M.: Efficient and stable large-area perovskite solar cells with inorganic charge extraction layers. *Science* **2015**(350), 944–948 (2015)
17. Wu, Y., Yang, X., Chen, W., Yue, Y., Cai, M., Xie, F., Bi, E., Islam, A., Han, L.: Perovskite solar cells with 18.21% efficiency and area over 1 cm<sup>2</sup> fabricated by heterojunction engineering. *Nat. Energy* **1**, 16148 (2016)
18. Mitzi, D., Feild, C., Harrison, W., Guloy, A.: Conducting tin halides with a layered organic-based perovskite structure. *Nature* **369**, 467–469 (1994)
19. Mitzi, D.B., Feild, C., Schlesinger, Z., Laibowitz, R.: Transport, optical, and magnetic properties of the conducting halide perovskite  $CH_3NH_3SnI_3$ . *J. Solid State Chem.* **114**, 159–163 (1995)
20. Kumar, M.H., Dharani, S., Leong, W.L., Boix, P.P., Prabhakar, R.R., Baikie, T., Shi, C., Ding, H., Ramesh, R., Asta, M.: Lead-free halide perovskite solar cells with high photocurrents realized through vacancy modulation. *Adv. Mater.* **26**, 7122–7127 (2014)
21. Eperon, G.E., Stranks, S.D., Menelaou, C., Johnston, M.B., Herz, L.M., Snaith, H.J.: Formamidinium lead trihalide: a broadly tunable perovskite for efficient planar heterojunction solar cells. *Energy Environ. Sci.* **7**, 982–988 (2014)
22. Hao, F., Stoumpos, C.C., Guo, P., Zhou, N., Marks, T.J., Chang, R.P., Kanatzidis, M.G.: Solvent-mediated crystallization of  $CH_3NH_3SnI_3$  films for heterojunction depleted perovskite solar cells. *J. Am. Chem. Soc.* **137**, 11445–11452 (2015)
23. Liao, W., Zhao, D., Yu, Y., Shrestha, N., Ghimire, K., Grice, C.R., Wang, C., Xiao, Y., Cimaroli, A.J., Ellingson, R.J.: Fabrication of efficient low-bandgap perovskite solar cells by combining formamidinium tin iodide with methylammonium lead iodide. *J. Am. Chem. Soc.* **138**, 12360–12363 (2016)
24. Wang, Z.K., Li, M., Yang, Y.G., Hu, Y., Ma, H., Gao, X.Y., Liao, L.S.: High efficiency Pb–In binary metal perovskite solar cells. *Adv. Mater.* **28**, 6695–6703 (2016)
25. Liao, W., Zhao, D., Yu, Y., Grice, C.R., Wang, C., Cimaroli, A.J., Schulz, P., Meng, W., Zhu, K., Xiong, R.G.: Lead-free inverted planar formamidinium tin triiodide perovskite solar cells achieving power conversion efficiencies up to 6.22%. *Adv. Mater.* **28**, 9333–9340 (2016)
26. Tsai, C.-M., Wu, H.-P., Chang, S.-T., Huang, C.-F., Wang, C.-H., Narra, S., Yang, Y.-W., Wang, C.-L., Hung, C.-H., Diao, E.W.-G.: Role of tin chloride in tin-rich mixed-halide perovskites applied as mesoscopic solar cells with a carbon counter electrode. *ACS Energy Lett.* **1**, 1086–1093 (2016)
27. Zhang, J., Shang, M.-H., Wang, P., Huang, X., Xu, J., Hu, Z., Zhu, Y., Han, L.: n-Type Doping and Energy States Tuning in  $CH_3NH_3Pb_{1-x}Sb_{2x/3}I_3$  Perovskite Solar Cells. *ACS Energy Lett.* **1**, 535–541 (2016)
28. Ogomi, Y., Morita, A., Tsukamoto, S., Saitho, T., Fujikawa, N., Shen, Q., Toyoda, T., Yoshino, K., Pandey, S.S., Ma, T.:  $CH_3NH_3Sn_xPb_{(1-x)}I_3$  perovskite solar cells covering up to 1060 nm. *J. Phys. Chem. Lett.* **5**, 1004–1011 (2014)
29. Stoumpos, C.C., Malliakas, C.D., Kanatzidis, M.G.: Semiconducting tin and lead iodide perovskites with organic cations: phase transitions, high mobilities, and near-infrared photoluminescent properties. *Inorg. Chem.* **52**, 9019–9038 (2013)
30. Kayesh, M.E., Chowdhury, T.H., Matsuishi, K., Kaneko, R., Kazzaoui, S., Lee, J.J., Noda, T., Islam, A.: Enhanced photovoltaic performance of  $FASnI_3$ -based perovskite solar cells with hydrazinium chloride coadditive. *ACS Energy Lett.* **3**(7), 1584–1589 (2018)
31. Hao, F., Stoumpos, C.C., Chang, R.P., Kanatzidis, M.G.: Anomalous band gap behavior in mixed Sn and Pb perovskites enables broadening of absorption spectrum in solar cells. *J. Am. Chem. Soc.* **136**, 8094–8099 (2014)
32. Yang, L., Cappel, U.B., Unger, E.L., Karlsson, M., Karlsson, K.M., Gabrielsson, E., Sun, L., Boschloo, G., Hagfeldt, A., Johansson, E.M.: Comparing spiro-OMeTAD and P3HT hole conductors in efficient solid state dye-sensitized solar cells. *Phys. Chem. Chem. Phys.* **14**, 779–789 (2012)
33. Zuo, F., Williams, S.T., Liang, P.W., Chueh, C.C., Liao, C.Y., Jen, A.K.Y.: Binary-metal perovskites toward high-performance planar-heterojunction hybrid solar cells. *Adv. Mater.* **26**, 6454–6460 (2014)
34. Chen, Q., Zhou, H., Fang, Y., Stieg, A.Z., Song, T.-B., Wang, H.-H., Xu, X., Liu, Y., Lu, S., You, J.: The optoelectronic role of chlorine in  $CH_3NH_3PbI_3(Cl)$ -based perovskite solar cells. *Nat. Commun.* **6**, 7269 (2015)
35. Docampo, P., Hanusch, F.C., Stranks, S.D., Döblinger, M., Feckl, J.M., Ehrensperger, M., Minar, N.K., Johnston, M.B., Snaith, H.J., Bein, T.: Solution deposition-conversion for planar heterojunction mixed halide perovskite solar cells. *Adv. Energy Mater.* **4**, 1400355 (2014)
36. Lee, S.J., Shin, S.S., Kim, Y.C., Kim, D., Ahn, T.K., Noh, J.H., Seo, J., Seok, S.I.: Fabrication of efficient formamidinium tin iodide perovskite solar cells through  $SnF_2$ -pyrazine complex. *J. Am. Chem. Soc.* **138**, 3974–3977 (2016)
37. Koh, T.M., Krishnamoorthy, T., Yantara, N., Shi, C., Leong, W.L., Boix, P.P., Grimsdale, A.C., Mhaisalkar, S.G., Mathews, N.: Formamidinium tin-based perovskite with low  $E_g$  for photovoltaic applications. *J. Mater. Chem. A* **3**, 14996–15000 (2015)
38. Koh, T.M., Fu, K., Fang, Y., Chen, S., Sum, T., Mathews, N., Mhaisalkar, S.G., Boix, P.P., Baikie, T.: Formamidinium-containing metal-halide: an alternative material for near-IR absorption perovskite solar cells. *J. Phys. Chem. C* **118**, 16458–16462 (2013)
39. Wetzelaer, G.J.A., Scheepers, M., Sempere, A.M., Momblona, C., Ávila, J., Bolink, H.J.: Trap-assisted non-radiative recombination in organic–inorganic perovskite solar cells. *Adv. Mater.* **27**, 1837–1841 (2015)
40. Yang, Z., Rajagopal, A., Jo, S.B., Chueh, C.-C., Williams, S., Huang, C.-C., Katahara, J.K., Hillhouse, H.W., Jen, A.K.-Y.:

- Stabilized wide bandgap perovskite solar cells by tin substitution. *Nano Lett.* **16**, 7739–7747 (2016)
41. Zhang, M., Lyu, M., Yu, H., Yun, J.H., Wang, Q., Wang, L.: Stable and low-cost mesoscopic CH<sub>3</sub>NH<sub>3</sub>PbI<sub>2</sub>Br perovskite solar cells by using a thin poly(3-hexylthiophene) layer as a hole transporter. *Chem. Eur. J.* **21**, 434–439 (2015)
  42. Colella, S., Mosconi, E., Fedeli, P., Listorti, A., Gazza, F., Orlandi, F., Ferro, P., Besagni, T., Rizzo, A., Calestani, G.: MAPbI<sub>3-x</sub>Cl<sub>x</sub> mixed halide perovskite for hybrid solar cells: the role of chloride as dopant on the transport and structural properties. *Chem. Mater.* **25**, 4613–4618 (2013)
  43. Yang, Z., Chueh, C.-C., Liang, P.-W., Crump, M., Lin, F., Zhu, Z., Jen, A.K.-Y.: Effects of formamidinium and bromide ion substitution in methylammonium lead triiodide toward high-performance perovskite solar cells. *Nano Energy* **22**, 328–337 (2016)
  44. Hu, M., Bi, C., Yuan, Y., Bai, Y., Huang, J.: Stabilized wide bandgap MAPbBr<sub>x</sub>I<sub>3-x</sub> perovskite by enhanced grain size and improved crystallinity. *Adv. Sci.* **3**(6), 1500301 (2016)
  45. Braly, I.L., Hillhouse, H.W.: Optoelectronic quality and stability of hybrid perovskites from MAPbI<sub>3</sub> to MAPbI<sub>2</sub>Br using composition spread libraries. *J. Phys. Chem. C* **120**, 893–902 (2016)
  46. Goldschmidt, V.M.: Die gesetze der krystallochemie. *Naturwissenschaften* **14**, 477–485 (1926)
  47. Hesse, S., Zimmermann, J., Von Seggern, H., Ehrenberg, H., Fuess, H., Fasel, C., Riedel, R.: CsEuBr 3: crystal structure and its role in the photostimulation of Cs Br:Eu<sup>2+</sup>. *J. Appl. Phys.* **100**, 083506 (2006)
  48. Shirwadkar, U., van Loef, E., Hawrami, R., Mukhopadhyay, S., Glodo, J., Shah, K.: New promising scintillators for gamma-ray spectroscopy: Cs (Ba,Sr)(Br,I)<sub>3</sub>. In: *IEEE Nuclear Science Symposium Conference Record*, 1583–1585 (2011)
  49. Stoumpos, C.C., Kanatzidis, M.G.: The renaissance of halide perovskites and their evolution as emerging semiconductors. *Acc. Chem. Res.* **48**, 2791–2802 (2015)
  50. Frolova, L.A., Anokhin, D.V., Gerasimov, K.L., Dremova, N.N., Troshin, P.A.: Exploring the effects of the Pb<sup>2+</sup> substitution in MAPbI<sub>3</sub> on the photovoltaic performance of the hybrid perovskite solar cells. *J. Phys. Chem. Lett.* **7**, 4353–4357 (2016)
  51. Zhang, W., Saliba, M., Moore, D.T., Pathak, S.K., Hörlantner, M.T., Stergiopoulos, T., Stranks, S.D., Eperon, G.E., Alexander-Webber, J.A., Abate, A.: Ultrasoft organic–inorganic perovskite thin-film formation and crystallization for efficient planar heterojunction solar cells. *Nat. Commun.* **6**, 6142 (2015)
  52. Unger, E.L., Bowring, A.R., Tassone, C.J., Pool, V.L., Gold-Parker, A., Cheacharoen, R., Stone, K.H., Hoke, E.T., Toney, M.F., McGehee, M.D.: Chloride in lead chloride-derived organometal halides for perovskite-absorber solar cells. *Chem. Mater.* **26**, 7158–7165 (2014)
  53. Colella, S., Mosconi, E., Pellegrino, G., Alberti, A., Guerra, V.L., Masi, S., Listorti, A., Rizzo, A., Condorelli, G.G., De Angelis, F.: Elusive presence of chloride in mixed halide perovskite solar cells. *J. Phys. Chem. Lett.* **5**, 3532–3538 (2014)
  54. Pérez-del-Rey, D., Forgács, D., Hutter, E.M., Savenije, T.J., Nordlund, D., Schulz, P., Berry, J.J., Sessolo, M., Bolink, H.J.: Strontium Insertion in methylammonium lead iodide: long charge carrier lifetime and high fill-factor solar cells. *Adv. Mater.* **28**, 9839–9845 (2016)
  55. Yin, W.J., Chen, H., Shi, T., Wei, S.H., Yan, Y.: Origin of high electronic quality in structurally disordered CH<sub>3</sub>NH<sub>3</sub>PbI<sub>3</sub> and the passivation effect of Cl and O at grain boundaries. *Adv. Electron. Mater.* **1**(6), 1500044 (2015)
  56. Zhao, W., Yang, D., Yang, Z., Liu, S.F.: Zn-doping for reduced hysteresis and improved performance of methylammonium lead iodide perovskite hybrid solar cells. *Mater. Today Energy* **5**, 205–213 (2017)
  57. Klug, M.T., Osherov, A., Haghghirad, A.A., Stranks, S.D., Brown, P.R., Bai, S., Wang, J.T.-W., Dang, X., Bulović, V., Snaith, H.J.: Tailoring metal halide perovskites through metal substitution: influence on photovoltaic and material properties. *Energy Environ. Sci.* **10**, 236–246 (2017)
  58. Heo, J.H., Han, H.J., Kim, D., Ahn, T.K., Im, S.H.: Hysteresis-less inverted CH<sub>3</sub>NH<sub>3</sub>PbI<sub>3</sub> planar perovskite hybrid solar cells with 18.1% power conversion efficiency. *Energy Environ. Sci.* **8**, 1602–1608 (2015)
  59. Xiao, Z., Bi, C., Shao, Y., Dong, Q., Wang, Q., Yuan, Y., Wang, C., Gao, Y., Huang, J.: Efficient, high yield perovskite photovoltaic devices grown by interdiffusion of solution-processed precursor stacking layers. *Energy Environ. Sci.* **7**, 2619–2623 (2014)
  60. Ahn, N., Son, D.-Y., Jang, I.-H., Kang, S.M., Choi, M., Park, N.-G.: Highly reproducible perovskite solar cells with average efficiency of 18.3% and best efficiency of 19.7% fabricated via Lewis base adduct of lead (II) iodide. *J. Am. Chem. Soc.* **137**, 8696–8699 (2015)
  61. Im, J.-H., Jang, I.-H., Pellet, N., Grätzel, M., Park, N.-G.: Growth of CH<sub>3</sub>NH<sub>3</sub>PbI<sub>3</sub> cuboids with controlled size for high-efficiency perovskite solar cells. *Nat. Nanotechnol.* **9**, 927–932 (2014)
  62. Qing, J., Chandran, H.-T., Cheng, Y.-H., Liu, X.-K., Li, H.-W., Tsang, S.-W., Lo, M.-F., Lee, C.-S.: Chlorine incorporation for enhanced performance of planar perovskite solar cell based on lead acetate precursor. *ACS Appl. Mater. Interfaces.* **7**, 23110–23116 (2015)
  63. Forgács, D., Sessolo, M., Bolink, H.J.: Lead acetate precursor-based pin perovskite solar cells with enhanced reproducibility and low hysteresis. *J. Mater. Chem. A* **3**, 14121–14125 (2015)
  64. Zhu, L., Yuh, B., Schoen, S., Li, X., Aldighaithir, M., Richardson, B.J., Alamer, A., Yu, Q.: Solvent-molecule-mediated manipulation of crystalline grains for efficient planar binary lead and tin triiodide perovskite solar cells. *Nanoscale* **8**, 7621–7630 (2016)
  65. Yang, Z., Rajagopal, A., Chueh, C.C., Jo, S.B., Liu, B., Zhao, T., Jen, A.K.-Y.: Stable low-bandgap Pb–Sn binary perovskites for tandem solar cells. *Adv. Mater.* **28**, 8990–8997 (2016)
  66. Liu, X., Yang, Z., Chueh, C.-C., Rajagopal, A., Williams, S.T., Sun, Y., Jen, A.K.-Y.: Improved efficiency and stability of Pb–Sn binary perovskite solar cells by Cs substitution. *J. Mater. Chem. A* **4**, 17939–17945 (2016)
  67. Liu, C., Fan, J., Li, H., Zhang, C., Mai, Y.: Highly efficient perovskite solar cells with substantial reduction of lead content. *Sci. Rep.* **6**, 35705 (2016)
  68. Li, Y., Sun, W., Yan, W., Ye, S., Rao, H., Peng, H., Zhao, Z., Bian, Z., Liu, Z., Zhou, H.: 50% Sn-based planar perovskite solar cell with power conversion efficiency up to 13.6%. *Adv. Energy Mater.* **6**, 1601353 (2016)
  69. Chen, Q., Chen, L., Ye, F., Zhao, T., Tang, F., Rajagopal, A., Jiang, Z., Jiang, S., Jen, A.K.-Y., Xie, Y.: Ag-incorporated organic–inorganic perovskite films and planar heterojunction solar cells. *Nano Lett.* **17**, 3231–3237 (2017)
  70. Ohishi, Y., Oku, T., Suzuki, A.: Fabrication and characterization of perovskite-based CH<sub>3</sub>NH<sub>3</sub>Pb<sub>1-x</sub>Ge<sub>x</sub>I<sub>3</sub>, CH<sub>3</sub>NH<sub>3</sub>Pb<sub>1-x</sub>Tl<sub>x</sub>I<sub>3</sub> and CH<sub>3</sub>NH<sub>3</sub>Pb<sub>1-x</sub>In<sub>x</sub>I<sub>3</sub> photovoltaic devices. *AIP Conf. Proc.* **1709**(1), 20020 (2016)
  71. Hamatani, T., Shirahata, Y., Ohishi, Y., Fukaya, M., Oku, T.: Arsenic and chlorine co-doping to CH<sub>3</sub>NH<sub>3</sub>PbI<sub>3</sub> perovskite solar cells. *Adv. Mater. Phys. Chem.* **7**(01), 1 (2017)
  72. Oku, T., Ohishi, Y., Suzuki, A.: Effects of SbBr 3 addition to CH<sub>3</sub>NH<sub>3</sub>PbI<sub>3</sub> solar cells. *AIP Conf Proc* **1807**(1), 020007 (2017)
  73. Eperon, G.E., Leijtens, T., Bush, K.A., Prasanna, R., Green, T., Wang, J.T.-W., McMeekin, D.P., Volonakis, G., Milot, R.L., May,



- R.: Perovskite-perovskite tandem photovoltaics with optimized band gaps. *Science* **354**, 861–865 (2016)
74. Zuo, C., Ding, L.: An 80.11% FF record achieved for perovskite solar cells by using the  $\text{NH}_4\text{Cl}$  additive. *Nanoscale* **6**, 9935–9938 (2014)
  75. Li, X., Bi, D., Yi, C., Décoppet, J.-D., Luo, J., Zakeeruddin, S.M., Hagfeldt, A., Grätzel, M.: A vacuum flash–assisted solution process for high-efficiency large-area perovskite solar cells. *Science* **353**(6294), 58–62 (2016)
  76. Saliba, M., Matsui, T., Domanski, K., Seo, J.-Y., Ummadisingu, A., Zakeeruddin, S.M., Correa-Baena, J.-P., Tress, W.R., Abate, A., Hagfeldt, A.: Incorporation of rubidium cations into perovskite solar cells improves photovoltaic performance. *Science* **354**, 206–209 (2016)
  77. Aharon, S., Cohen, B.E., Etgar, L.: Hybrid lead halide iodide and lead halide bromide in efficient hole conductor free perovskite solar cell. *J. Phys. Chem. C* **118**, 17160–17165 (2014)
  78. Wehrenfennig, C., Eperon, G.E., Johnston, M.B., Snaith, H.J., Herz, L.M.: High charge carrier mobilities and lifetimes in organolead trihalide perovskites. *Adv. Mater.* **26**, 1584–1589 (2014)
  79. Hao, F., Stoumpos, C.C., Cao, D.H., Chang, R.P., Kanatzidis, M.G.: Lead-free solid-state organic–inorganic halide perovskite solar cells. *Nat. Photonics* **8**, 489–494 (2014)
  80. Nie, W., Tsai, H., Asadpour, R., Blancon, J.-C., Neukirch, A.J., Gupta, G., Crochet, J.J., Chhowalla, M., Tretiak, S., Alam, M.A.: High-efficiency solution-processed perovskite solar cells with millimeter-scale grains. *Science* **347**, 522–525 (2015)
  81. Kim, H.-B., Choi, H., Jeong, J., Kim, S., Walker, B., Song, S., Kim, J.Y.: Mixed solvents for the optimization of morphology in solution-processed, inverted-type perovskite/fullerene hybrid solar cells. *Nanoscale* **6**, 6679–6683 (2014)
  82. Yang, W.S., Noh, J.H., Jeon, N.J., Kim, Y.C., Ryu, S., Seo, J., Seok, S.I.: High-performance photovoltaic perovskite layers fabricated through intramolecular exchange. *Science* **348**, 1234–1237 (2015)
  83. Meillaud, F., Shah, A., Droz, C., Vallat-Sauvain, E., Miazza, C.: Efficiency limits for single-junction and tandem solar cells. *Solar Energy Mater. Solar Cells* **90**(18–19), 2952–2959 (2006)
  84. Ke, W., Stoumpos, C.C., Logsdon, J.L., Wasielewski, M.R., Yan, Y., Fang, G., Kanatzidis, M.G.:  $\text{TiO}_2$ – $\text{ZnS}$  cascade electron transport layer for efficient formamidinium tin iodide perovskite solar cells. *J. Am. Chem. Soc.* **138**, 14998–15003 (2016)
  85. Gur, I., Fromer, N.A., Geier, M.L., Alivisatos, A.P.: Air-stable all-inorganic nanocrystal solar cells processed from solution. *Science* **310**, 462–465 (2005)
  86. Shin, B., Gunawan, O., Zhu, Y., Bojarczuk, N.A., Chy, S.J., Guha, S.: Thin film solar cell with 8.4% power conversion efficiency using an earth-abundant  $\text{Cu}_2\text{ZnSnS}_4$  absorber. *Prog. Photovolt. Res. Appl.* **21**, 72–76 (2013)
  87. Chuang, C.-H.M., Brown, P.R., Bulović, V., Bawendi, M.G.: Improved performance and stability in quantum dot solar cells through band alignment engineering. *Nat. Mater.* **13**, 796 (2014)
  88. Chen, L.-J., Lee, C.-R., Chuang, Y.-J., Wu, Z.-H., Chen, C.: Synthesis and optical properties of lead-free cesium tin halide perovskite quantum rods with high-performance solar cell application. *J. Phys. Chem. Lett.* **7**, 5028–5035 (2016)
  89. Biswas, A., Bayer, I.S., Biris, A.S., Wang, T., Dervishi, E., Faupel, F.: Advances in top–down and bottom–up surface nanofabrication: techniques, applications & future prospects. *Adv. Colloid Interface Sci.* **170**, 2–27 (2012)
  90. Cavallini, M., Facchini, M., Massi, M., Biscarini, F.: Bottom–up nanofabrication of materials for organic electronics. *Synth. Metals* **146**, 283–286 (2004)
  91. Ariga, K., Hill, J.P., Ji, Q.: Layer-by-layer assembly as a versatile bottom-up nanofabrication technique for exploratory research and realistic application. *Phys. Chem. Chem. Phys.* **9**, 2319–2340 (2007)
  92. Green, M.A., Ho-Baillie, A., Snaith, H.J.: The emergence of perovskite solar cells. *Nat. Photonics* **8**, 506–514 (2014)
  93. Miller, O.D., Yablonovitch, E., Kurtz, S.R.: Strong internal and external luminescence as solar cells approach the Shockley-Queisser limit. *IEEE J. Photovolt.* **2**, 303–311 (2012)
  94. Krishnamoorthy, T., Ding, H., Yan, C., Leong, W.L., Baikie, T., Zhang, Z., Sherburne, M., Li, S., Asta, M., Mathews, N.: Lead-free germanium iodide perovskite materials for photovoltaic applications. *J. Mater. Chem. A* **3**, 23829–23832 (2015)
  95. Fabian, D.M., Ardo, S.: Hybrid organic–inorganic solar cells based on bismuth iodide and 1, 6-hexanediammonium dication. *J. Mater. Chem. A* **4**, 6837–6841 (2016)
  96. Yokoyama, T., Cao, D.H., Stoumpos, C.C., Song, T.-B., Sato, Y., Aramaki, S., Kanatzidis, M.G.: Overcoming short-circuit in lead-free  $\text{CH}_3\text{NH}_3\text{SnI}_3$  perovskite solar cells via kinetically controlled gas-solid reaction film fabrication process. *J. Phys. Chem. Lett.* **7**, 776–782 (2016)
  97. Zhang, M., Lyu, M., Yun, J.-H., Noori, M., Zhou, X., Cooling, N.A., Wang, Q., Yu, H., Dastoor, P.C., Wang, L.: Low-temperature processed solar cells with formamidinium tin halide perovskite/fullerene heterojunctions. *Nano Res.* **9**, 1570–1577 (2016)
  98. Gupta, S., Bendikov, T., Hodes, G., Cahen, D.:  $\text{CsSnBr}_3$ , a lead-free halide perovskite for long-term solar cell application: insights on  $\text{SnF}_2$  addition. *ACS Energy Lett.* **1**, 1028–1033 (2016)
  99. Hsu, H.-Y., Ji, L., Du, M., Zhao, J., Edward, T.Y., Bard, A.J.: Optimization of lead-free organic–inorganic tin (II) halide perovskite semiconductors by scanning electrochemical microscopy. *Electrochim. Acta* **220**, 205–210 (2016)
  100. Yu, Y., Zhao, D., Grice, C.R., Meng, W., Wang, C., Liao, W., Cimaroli, A.J., Zhang, H., Zhu, K., Yan, Y.: Thermally evaporated methylammonium tin triiodide thin films for lead-free perovskite solar cell fabrication. *RSC Adv.* **6**, 90248–90254 (2016)
  101. Jung, M.-C., Raga, S.R., Qi, Y.: Properties and solar cell applications of Pb-free perovskite films formed by vapor deposition. *RSC Adv.* **6**, 2819–2825 (2016)
  102. Song, T.-B., Yokoyama, T., Stoumpos, C.C., Logsdon, J.L., Cao, D.H., Wasielewski, M.R., Aramaki, S., Kanatzidis, M.G.: Importance of reducing vapor atmosphere in the fabrication of tin-based perovskite solar cells. *J. Am. Chem. Soc.* **139**(2), 836–842 (2017)
  103. Li, W., Li, J., Li, J., Fan, J., Mai, Y., Wang, L.: Additive-assisted construction of all-inorganic  $\text{CsSnI}_2\text{Br}$  2 mesoscopic perovskite solar cells with superior thermal stability up to 473 K. *J. Mater. Chem. A* **4**, 17104–17110 (2016)
  104. Qiu, X., Cao, B., Yuan, S., Chen, X., Qiu, Z., Jiang, Y., Ye, Q., Wang, H., Zeng, H., Liu, J.: From unstable  $\text{CsSnI}_3$  to air-stable  $\text{Cs}_2\text{SnI}_6$ : a lead-free perovskite solar cell light absorber with bandgap of 1.48 eV and high absorption coefficient. *Sol. Energy Mater. Sol. Cells* **159**, 227–234 (2017)
  105. Sourisseau, S., Louvain, N., Bi, W., Mercier, N., Rondeau, D., Boucher, F., Buzaré, J.-Y., Legein, C.: Reduced band gap hybrid perovskites resulting from combined hydrogen and halogen bonding at the organic–inorganic interface. *Chem. Mater.* **19**, 600–607 (2007)
  106. Takahashi, Y., Obara, R., Nakagawa, K., Nakano, M., Tokita, J.-Y., Inabe, T.: Tunable charge transport in soluble organic–inorganic hybrid semiconductors. *Chem. Mater.* **19**, 6312–6316 (2007)
  107. Knutson, J.L., Martin, J.D., Mitzi, D.B.: Tuning the band gap in hybrid tin iodide perovskite semiconductors using structural templating. *Inorg. Chem.* **44**, 4699–4705 (2005)

## Affiliations

Mohd Aizat A. Wadi<sup>1,2</sup> · Towhid H. Chowdhury<sup>1,3</sup> · Idriss M. Bedja<sup>4</sup> · Jae-Joon Lee<sup>3</sup> · Nowshad Amin<sup>5</sup> · Md. Aktharuzzaman<sup>2</sup> · Ashraful Islam<sup>1</sup> 

✉ Jae-Joon Lee  
jjlee@dongguk.edu

✉ Md. Aktharuzzaman  
akhtar@ukm.edu.my

✉ Ashraful Islam  
ISLAM.Ashraful@nims.go.jp

<sup>1</sup> Photovoltaic Materials Group, Center for Green Research on Energy and Environmental Materials, National Institute for Material Science, 1-2-1, Sengen, Tsukuba, Ibaraki 305-0047, Japan

<sup>2</sup> Solar Energy Research Institute (SERI), Universiti Kebangsaan Malaysia (UKM), 43600 Bangi, Selangor, Malaysia

<sup>3</sup> Department of Energy and Materials Engineering & Research Center for Photoenergy Harvesting and Conversion Technology (phct), Dongguk University, Seoul 04620, Republic of Korea

<sup>4</sup> Cornea Research Center, Optometry Department, College of Applied Medical Sciences, King Saud University, Riyadh 11433, Saudi Arabia

<sup>5</sup> Institute of Sustainable Energy (ISE), Universiti Tenaga Nasional (@The National Energy University), Jalan IKRAM-UNITEN, 43000 Kajang, Selangor, Malaysia